THE ASTROPHYSICAL JOURNAL, 335:239–262, 1988 December 1

EQUILIBRIA AND EVOLUTIONS OF MAGNETIZED, ROTATING, ISOTHERMAL CLOUDS. II. THE EXTREME CASE: NONROTATING CLOUDS

KOHJI TOMISAKA
Faculty of Education, Niigata University

SATORU IKEUCHI
National Astronomical Observatory

AND

TAKASHI NAKAMURA
Department of Physics, Kyoto University

Received 1988 January 22; accepted 1988 May 18

ABSTRACT

Structures of nonrotating magnetized clouds are investigated from a standpoint of the equilibrium solution of the cloud confined by an external pressure which is threaded by uniform magnetic field at infinity. Equilibria for wide ranges of parameters are studied: the ratio of the external thermal pressure to the magnetic pressure ranges from 10^{-2} to 5 and the center-to-surface density ratio ranges from 2 to 10^4. We obtain two different equilibrium states with the same mass but with different central density. It is shown from the mass–central density relation that the solution with lower central density is stable and that with higher central density is unstable. The maximum mass of clouds ($M_{\rm cr}$) supported by a fixed magnetic flux is well approximated by the mass-to-flux ratio at the cloud center ($dm/d\Phi_B|_{r=0}$):

$$M_{\rm cr} \simeq 62\left\{1 - \left[\frac{0.17}{dm/d(\Phi_B/G^{1/2})|_{r=0}}\right]^2\right\}^{-3/2} \frac{c_s^4}{p_{\rm ext}^{1/2}(4\pi G)^{3/2}},$$

where $p_{\rm ext}$ and c_s represent the external pressure and the isothermal sound speed in the cloud. Effects of the distribution of magnetic flux on the equilibrium structure are also studied. We show that the thin-disk approximation is successfully applied to the magnetized cloud, if magnetic fields are strong enough. It is suggested that there are two possibilities for the initiation of star formation, i.e., that the mass of cloud exceeds $M_{\rm cr}$ and that the cloud is compressed beyond the unstable equilibrium solution with higher central density.

Subject headings: hydromagnetics — interstellar: magnetic fields — nebulae: general — nebulae: internal motions

I. INTRODUCTION

Several examples have been found of an infrared (IR) source and associated bipolar outflow occurring at the center of the disk cloud. The circumstellar or circum-outflow disks are observed in, e.g., L1551–IRS 5, OMC-1-KL, NGC 2071–IRS, R Mon, NGC 6334 V, and S106 (Harvey 1985), whose typical sizes are 0.1–1 pc. Further, clumps in molecular clouds often show an elongated shape (Heyer *et al.* 1987). Such disk configurations seem to be due to the presence of magnetic field and/or rotation. That is, clouds are supported laterally by the magnetic pressure and tension and/or the centrifugal force.

In the Taurus molecular cloud, the direction of the magnetic field which is measured by the polarization of background stars (near-IR: Tamura *et al.* 1987; optical wavelengths: Heyers *et al.* 1987) is parallel to the minor axes of the clumps. The observational results suggest that the cloud collapse is controlled by the magnetic field, although the field strength is not accurately measured. Zeeman splitting of thermal OH allows the measurement of the field strength $B_{\parallel}$ in the region with density above 10^3 cm^{-3} as 10–100 μG (Heiles 1987).

The disk clouds and clumps can be considered as in (magneto-)hydrostatic equilibrium, at least in quasi-equilibrium. The exact equilibrium configuration of the isothermal cloud supported by a magnetic field has been obtained numerically by Mouschovias (1976*a*, *b*). In his model a spherical "parent cloud" with uniform density ρ_i, radius $R_{\rm cl}$, and mass $M_{\rm cl} = (4\pi/3)\rho_i R_{\rm cl}^3$ is threaded by a uniform magnetic field $\boldsymbol{B}_0$, and this "parent cloud" collapses, keeping flux freezing, to be the final equilibrium solution. The maximum mass of the cloud laterally supported by the magnetic field, $M_{\rm cr}$, is obtained as the mass above which solutions are not found. This mass is expressed approximately using the magnetic flux anchored to the cloud, $(\Phi_B)_{\rm cl} \equiv \pi R_{\rm cl}^2 B_0$ (Mouschovias and Spitzer 1976), as

$$M_{\rm cr} \simeq 1.37\left[1 - 0.016\,\frac{(\Phi_B)_{\rm cl}^2/G}{M_{\rm cr}^2}\right]^{-3/2} \frac{c_s^4}{G^{3/2}p_{\rm ext}^{1/2}}, \quad (1.1)$$

where c_s, $p_{\rm ext}$, and G represent the isothermal sound speed, the external pressure, and the gravitational constant, respectively. Another method of obtaining the equilibrium configuration was introduced by Mestel and Ray (1985), in which, for a given gravitational potential, the initial mass and magnetic field distributions are determined to counterbalance the gravity.

Pioneering work by Mouschovias (1976*a*, *b*) has some restrictions because relatively large numerical calculations were needed: a shape of the "parent cloud" (spherical) and the distribution of magnetic field (uniform) are fixed, and the examined ranges of parameters (e.g., center-to-surface density ratio, $2 \lesssim \rho_c/\rho_s \lesssim 30$) are relatively limited. We presented the method of obtaining the equilibrium solution of a magnetized, rotating, isothermal cloud in the case of poloidal magnetic fields parallel to the rotation axis (Tomisaka, Ikeuchi, and

Nakamura 1988, hereafter Paper I). In a present paper, we pay attention to the effect of magnetic field and confine ourselves to the equilibrium configurations of *nonrotating* clouds as a first step to more general cases including rotation.

We present the results for various shapes and magnetic field distributions of the "parent cloud." Comparing the results with different mass distributions $m(\Phi_B)$, we can see the stability of the cloud when $m(\Phi_B)$ is changed, as a result, for example, of the plasma drift (ambipolar diffusion) or cloud-cloud collision.

In order to see the stability of the cloud in equilibrium briefly, it is convenient to find an $M_{\rm cl}$-ρ_c relation (Tassoul 1978), i.e., the solution with $\partial M_{\rm cl}/\partial \rho_c > 0$ is stable and that with $\partial M_{\rm cl}/\partial \rho_c < 0$ is unstable. We present in § III the $M_{\rm cl}$-ρ_c relation for equilibrium structures of magnetically supported clouds and check the stability condition for various *equilibrium* solutions. From the $M_{\rm cl}$-ρ_c relation, we can also determine exactly the maximum mass above which no equilibrium solutions exist.

Further, to see the solutions with wide ranges of parameters, we take the ratio of the external pressure to the magnetic pressure of the initial uniform field, $\beta_0 \equiv p_{\rm ext}/(B_0^2/8\pi)$, from 10^{-2} to 5.

The plan of this paper is as follows: in § II we briefly describe the method of obtaining the solution. Numerical results are shown in § III. It is shown in § IV that the results are qualitatively explained by the analysis of the Gibbs free energy of a homogeneous spherical cloud. The relation between the stability of magnetized clouds and star formation is also discussed in § IV. Section V is devoted to the summary of the paper.

II. METHOD

The method for calculating equilibrium solutions of a self-gravitating, isothermal, axisymmetric cloud without rotation is essentially the same as that presented by Mouschovias (1976*a*). The formulation which includes the effect of rotation (Paper I) is also valid for the nonrotating case when we put an angular rotation speed of zero, $\Omega_{\rm cl} = 0$. Here we briefly summarize the method.

1. Along the direction of the magnetic field, the magnetohydrostatic equilibrium is expressed by setting $\Omega = 0$ in equation (I.2.19) (eq. [I.2.19] is eq. [2.19] of Paper I), as

$$\rho = \frac{q(\Phi)}{c_s^2} \exp\left(-\frac{\psi}{c_s^2}\right), \tag{2.1}$$

where ρ, ψ, and Φ represent, respectively, the density, the gravitational potential, and the magnetic potential, which is related to the magnetic flux Φ_B as $\Phi = \Phi_B/(2\pi)$, and $q(\Phi)$ is an integration constant depending only on Φ.

2. On the other hand, in the direction perpendicular to the magnetic field, from equation (I.2.1) the magnetohydrostatic equation has the form

$$-\frac{1}{4\pi r^2} \Delta_1 \Phi(\hat{e}_\phi \times \boldsymbol{B}) - \rho\nabla\psi - c_s^2 \nabla\rho = 0 , \tag{2.2}$$

where $\Delta_1 \equiv \partial^2/\partial z^2 + r(\partial/\partial r)[(1/r)(\partial/\partial r)]$.

3. We can rewrite equation (2.2) using equations (2.1), (I.2.5), and (I.2.6), as

$$\Delta_1 \Phi = -4\pi r^2 \frac{dq(\Phi)}{d\Phi} \exp\left(-\frac{\psi}{c_s^2}\right). \tag{2.3}$$

This is an equation to determine the magnetic field. The Poisson equation to determine the gravitational potential is expressed as

$$\nabla^2 \psi = 4\pi G \frac{q(\Phi)}{c_s^2} \exp\left(-\frac{\psi}{c_s^2}\right). \tag{2.4}$$

By solving equations (2.3) and (2.4) simultaneously, equilibrium solutions of a self-gravitating, isothermal, magnetized cloud is obtained.

The function $q(\Phi)$ is given by setting the mass in a flux tube equal to that in a "parent cloud" (eq. [I.2.30a]). Several cases of the distribution of mass with magnetic flux are examined. We consider that uniform magnetic fields parallel to the z-direction thread the uniform-density "parent cloud" with various shapes. To express the shape simply, we extend equation (I.2.31a) as

$$\frac{dm}{d\Phi} = \left(\frac{N}{2} + 1\right) \frac{M_{\rm cl}}{\Phi_{\rm cl}} \left(1 - \frac{\Phi}{\Phi_{\rm cl}}\right)^{N/2}, \tag{2.5}$$

with

$$\Phi_{\rm cl} = \frac{(\Phi_B)_{\rm cl}}{2\pi} \equiv \frac{R_{\rm cl}^2 B_0}{2}. \tag{2.6}$$

We study the three cases $N = 0$, 1, and 2. In the case of $N = 0$, the "parent cloud" is cylindrical. The cases with $N = 1$ and $N = 2$ correspond respectively to the spherical "parent cloud" and that whose surface is a paraboloid. With increasing N, the central concentration of the column density along the z-direction, σ, increases. That is, for $N = 0$, σ/B_0 is constant irrespective of r, and for $N \geq 1$, σ/B_0 increases with decreasing r. Therefore, the last case ($N = 2$) will be called that of the "centrally condensed parent cloud."

Parameters which characterize the solution are $R_{\rm cl}$, the radius of the "parent cloud"; β_0, the ratio of the external thermal pressure $p_{\rm ext}$ to the magnetic pressure $B_0^2/8\pi$; and ρ_c/ρ_s, the center-to-surface density ratio of the solution. Using the normalization in equation (I.2.34),[1] we use the central density ρ_c as the third parameter.

We solve numerically equations (2.3) and (2.4) simultaneously under an appropriate boundary condition (I.2.42) by the self-consistent field method. The numerical scheme is the same as described in § III of Paper I, but we employ the checkerboard successive overrelaxation (SOR) method instead of ordinary SOR to solve equations (2.3) and (2.4) to improve the vectorization of the numerical scheme. The number of numerical meshes is taken as 80 in the z-direction and as 40 in the r-direction. The outer boundary where the boundary conditions (I.2.42) are set is placed at $r = (2\text{–}2.3) \times R_{\rm cl}$ and $z = (2.1\text{–}2.5) \times R_{\rm cl}$.

III. NUMERICAL RESULTS

a) Sequence of Solutions for Changing ρ_c

In § IV of Paper I, we have shown a sequence of solutions with the same ρ_c but different β_0. In this subsection, the solutions with the same β_0 but different ρ_c are presented. From this, we can find the $M_{\rm cl}$-ρ_c relation and obtain information on the stability of the equilibrium.

First, we confine ourselves to the spherical "parent cloud" ($N = 1$), and in § III*d* we compare with the cylindrical ($N = 0$) and centrally condensed ($N = 2$) clouds. Figure 1 shows the

[1] There are typographical errors in equation (I.2.34). As easily noticed, Ω should be normalized as $\Omega/(4\pi G\rho_c)^{1/2}$.

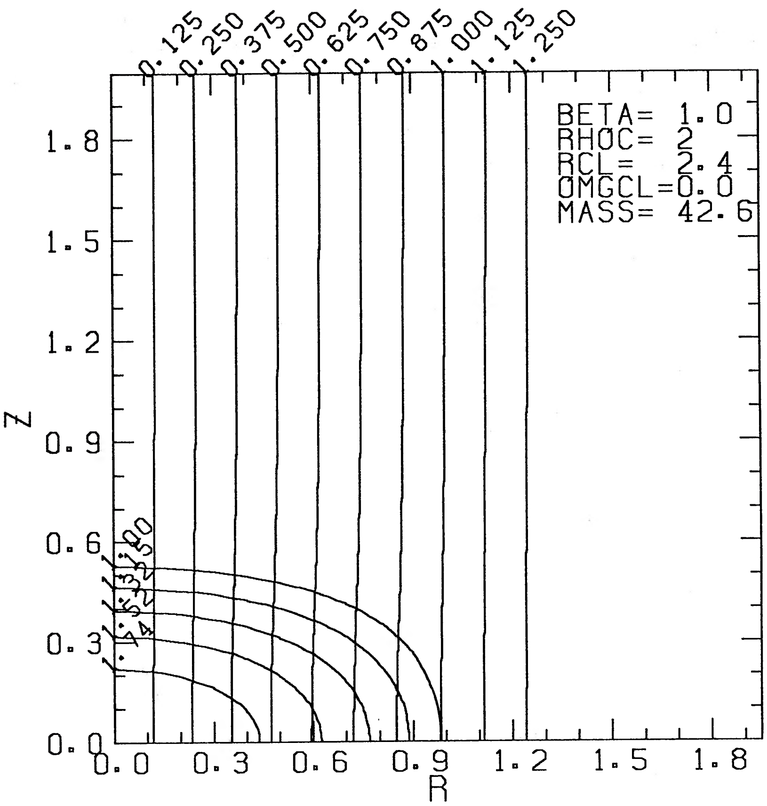

FIG. 1*a*

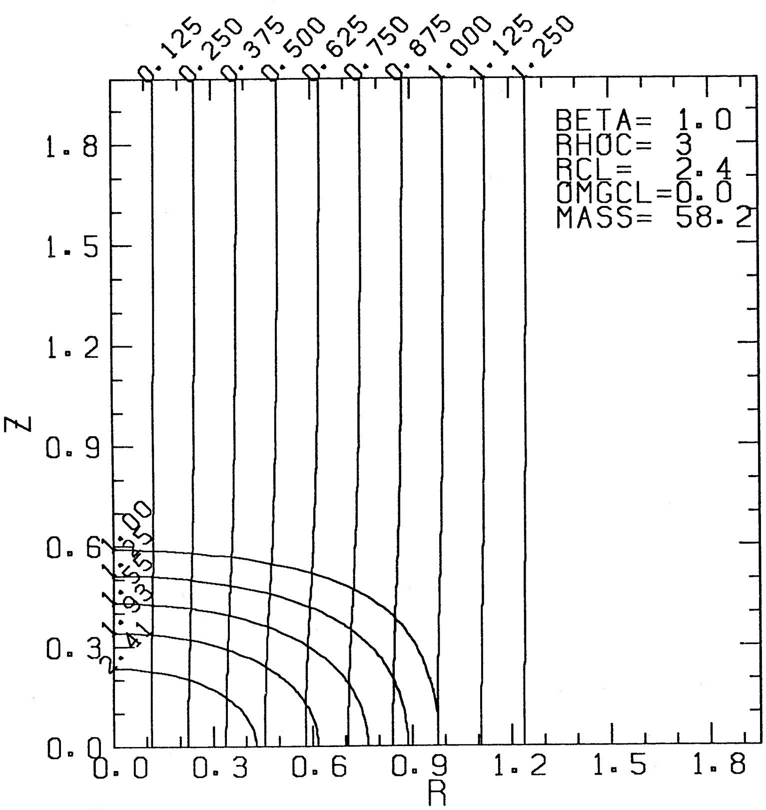

FIG. 1*b*

FIG. 1.—Equilibrium configurations of magnetized clouds with $R_{cl} = 2.4$ and $\beta_0 = 1$. The magnetic field line, which runs almost vertically, and the density contour are plotted. Each magnetic field line is labeled by the radius where the magnetic field runs far from the cloud ($z = \infty$). The contour level of the density, which is taken as $\log \rho = [(\log \rho_c)/5]n$, for $n = 0$–4, is also shown near the contour line. The horizontal and vertical axis mean, respectively, the normalized distance as r/R_{cl} and z/R_{cl}. Parameters used here are shown in Table 1.

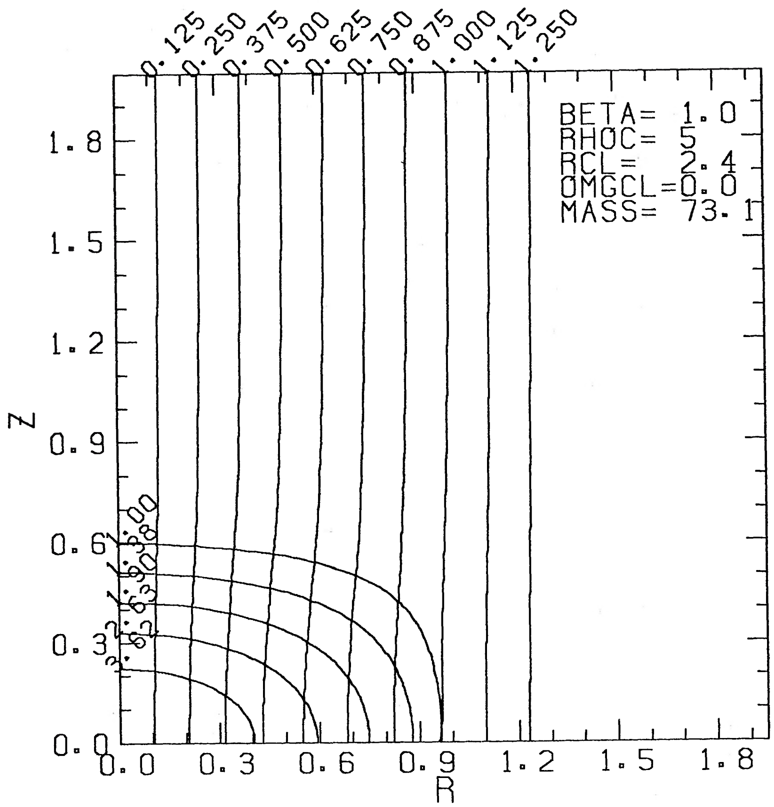
0.125
0.250
0.375
0.500
0.625
0.750
0.875
1.000
1.125
1.250
BETA= 1.0
RHOC= 5
RCL= 2.4
OMGCL=0.0
MASS= 73.1
1.8
1.5
1.2
Z
0.9
0.6
0.3
0.0
0.0
0.3
0.6
0.9
1.2
1.5
1.8
R

FIG. 1c

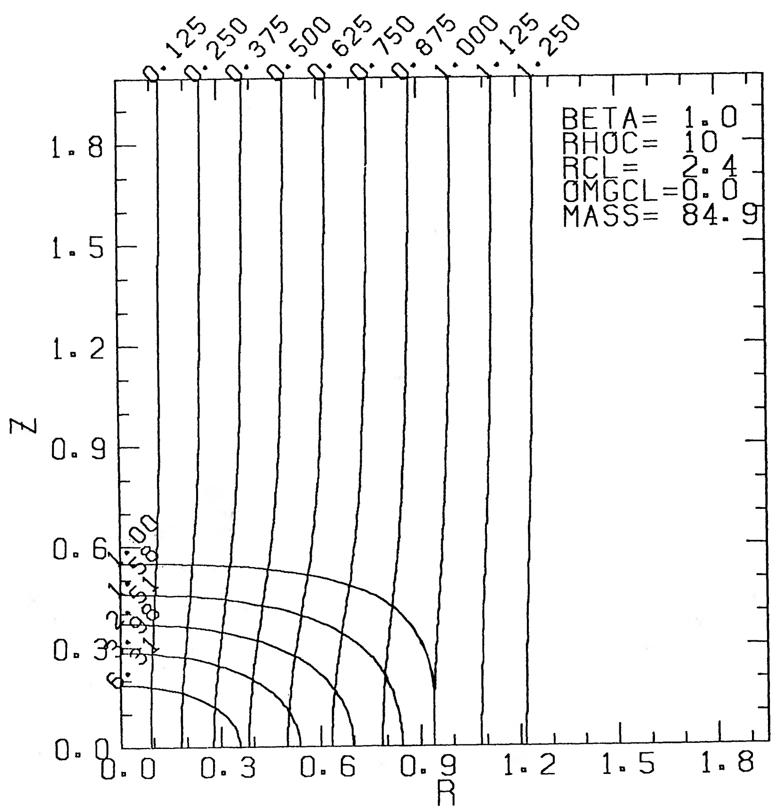
0.125
0.250
0.375
0.500
0.625
0.750
0.875
1.000
1.125
1.250
BETA= 1.0
RHOC= 10
RCL= 2.4
OMGCL=0.0
MASS= 84.9
1.8
1.5
1.2
Z
0.9
0.6
0.3
0.0
0.0
0.3
0.6
0.9
1.2
1.5
1.8
R

FIG. 1d

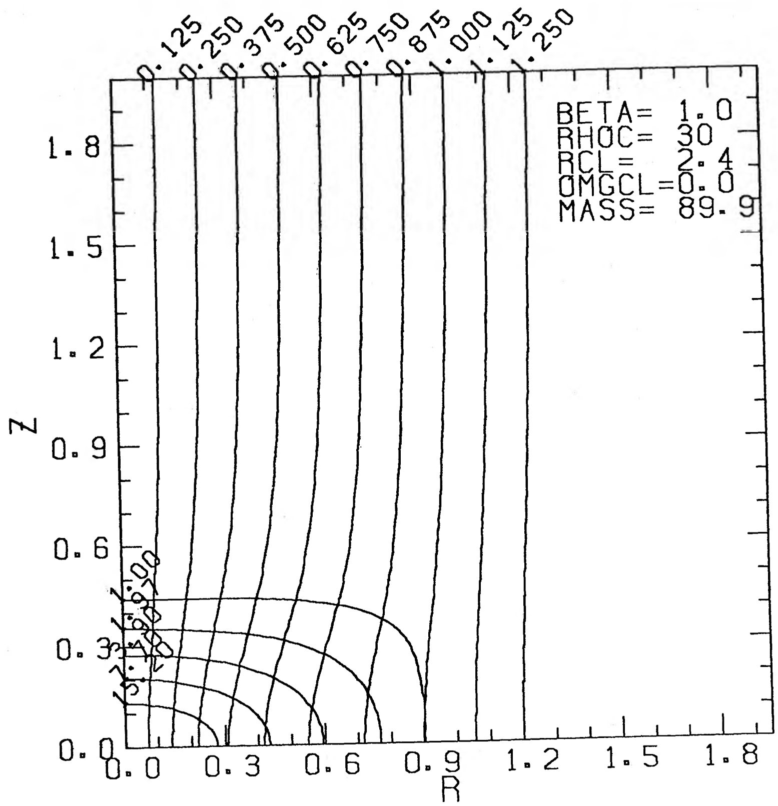
0.125
0.250
0.375
0.500
0.625
0.750
0.875
1.000
1.125
1.250
BETA= 1.0
RHOC= 30
RCL= 2.4
OMGCL=0.0
MASS= 89.9
Z
R

FIG. 1*e*

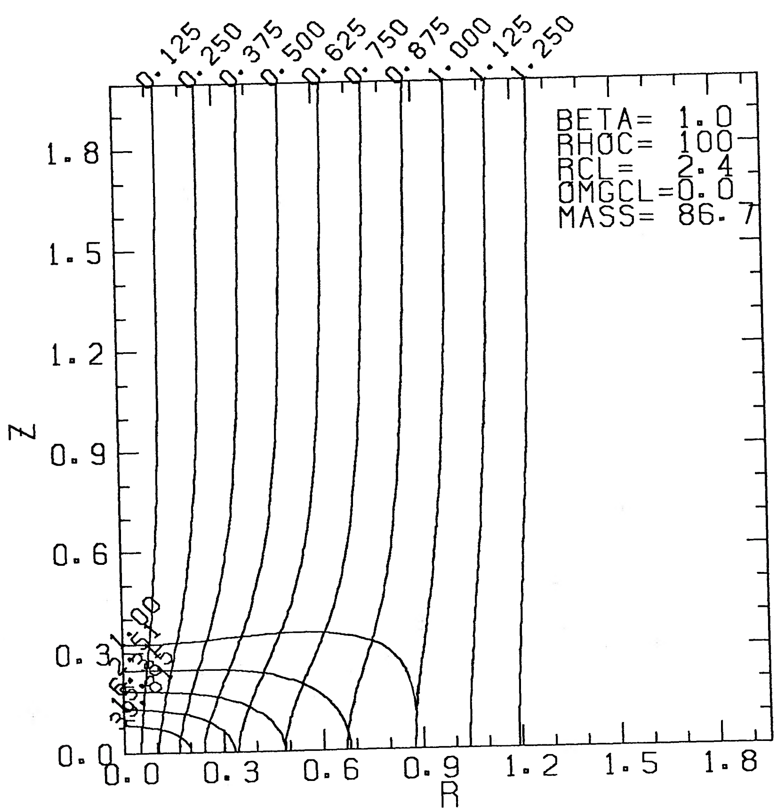
0.125
0.250
0.375
0.500
0.625
0.750
0.875
1.000
1.125
1.250
BETA= 1.0
RHOC= 100
RCL= 2.4
OMGCL=0.0
MASS= 86.7
Z
R

FIG. 1*f*

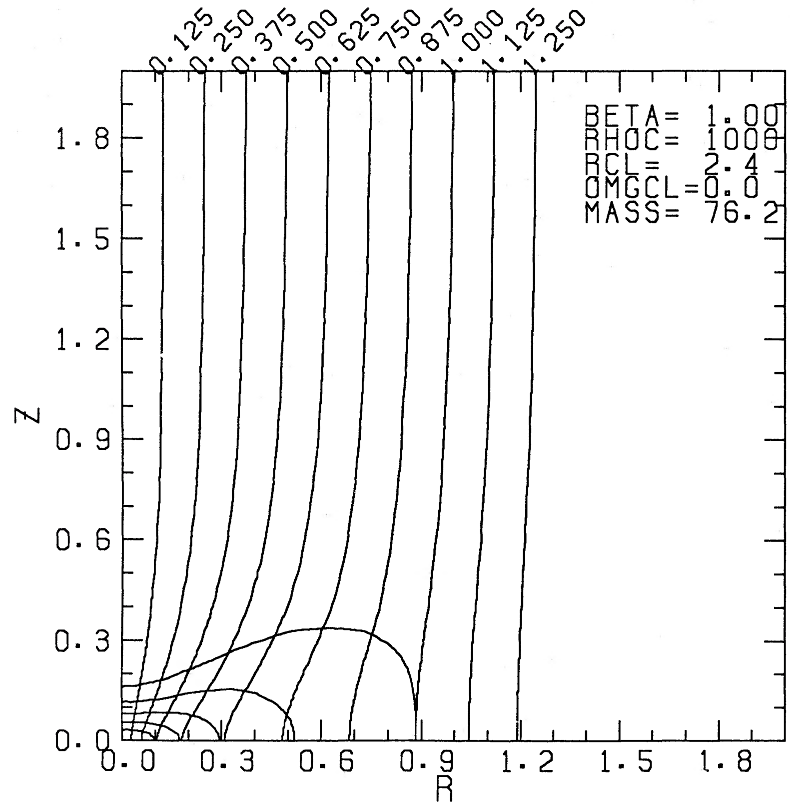
0.125 0.250 0.375 0.500 0.625 0.750 0.875 1.000 1.125 1.250
BETA= 1.00
RHOC= 1000
RCL= 2.4
OMGCL=0.0
MASS= 76.2
Z
R
0.0 0.3 0.6 0.9 1.2 1.5 1.8

FIG. 1*g*

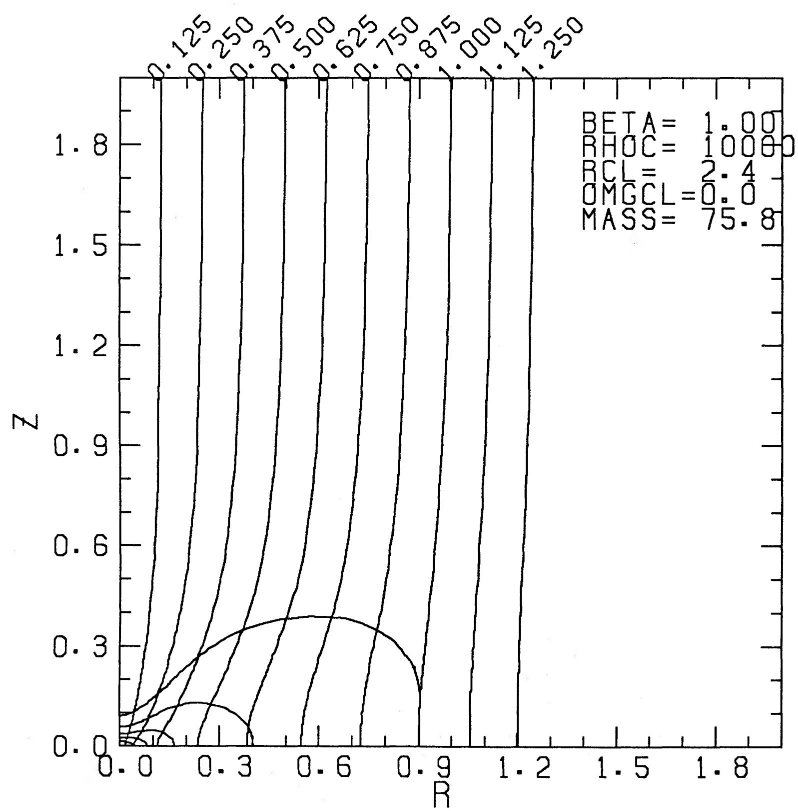
0.125 0.250 0.375 0.500 0.625 0.750 0.875 1.000 1.125 1.250
BETA= 1.00
RHOC= 10000
RCL= 2.4
OMGCL=0.0
MASS= 75.8
Z
R
0.0 0.3 0.6 0.9 1.2 1.5 1.8

FIG. 1*h*

solutions with fixed $R_{cl} = 2.4$ and $\beta_0 = 1$, but the central density ρ_c changes from 2 to 10^4. When the central density is as low as $\rho_c \lesssim 30$, the cloud keeps its shape spheroidal, that is, the cloud seems to collapse along the z-direction from the parent cloud. The spheroidal shape clearly shows the lateral support by the magnetic field. When ρ_c exceeds ~ 50, the cloud changes to the concave shape. The height of the cloud on the z-axis, Z_{fin}, decreases for higher central concentration. The ratio of the height Z_{fin} to the radius R_{fin} on the r-axis increases from 0.53 ($\rho_c = 2$) to 0.62 ($\rho_c = 5$), and then decreases to 0.056 ($\rho_c = 10^4$).

The appearance of the concave shape for high ρ_c is explained as follows: the density distribution in the z-direction can be approximated by the uniform thin disk extending infinitely in the r-direction (thin-disk approximation). Then the half-thickness is given (Kiguchi *et al.* 1987) by

$$z_b = 2^{1/2} \frac{\ln [\rho_c^{1/2} + (\rho_c - 1)^{1/2}]}{\rho_c^{1/2}} , \quad (3.1)$$

which decreases for $\rho_c \geq 3.28$ with an increase in ρ_c from $z_b(\rho_c = 10) = 0.471$ to $z_b(\rho_c = 10^4) = 0.075$. On the other hand, the height of the cloud at $r \neq 0$ is also expressed approximately by replacing ρ_c by $\rho(z = 0, r)$ in equation (3.1). Then if $\rho_c > \rho(z = 0, r) \gtrsim 5$, equation (3.1) indicates that $z_b(r > 0) > z_b(r = 0)$.

In Figure 2 we plot the density distribution at the equatorial plane ($z = 0$) against the radial distance from the z-axis. As long as the central density is low ($\rho_c \simeq 10$), the density distribution reflects the initial mass distribution varying as $[1 - (r/R_{cl})^2]^{1/2}$ (eq. [2.5]). As the central density increases, the density distribution approaches gradually that proportional to r^{-2}. Such circumstances resemble the cases of an isothermal nonmagnetized self-gravitating sphere (Shu 1977). This shows that the pressure gradient is more important than the magnetic force. Kiguchi *et al.* (1987) have also pointed out that the rotating isothermal self-gravitating cloud shows a density distribution proportional to r^{-2} in the case with large central concentration ($\rho_c/\rho_s \gg 1$). As for the former case, in the limit of infinite central concentration, the equilibrium density distribution, which is unstable, approaches a "singular" distribution (Chandrasekhar 1957) as $\rho(r) = c_s^2/(2\pi G)r^{-2}$. In this case, the

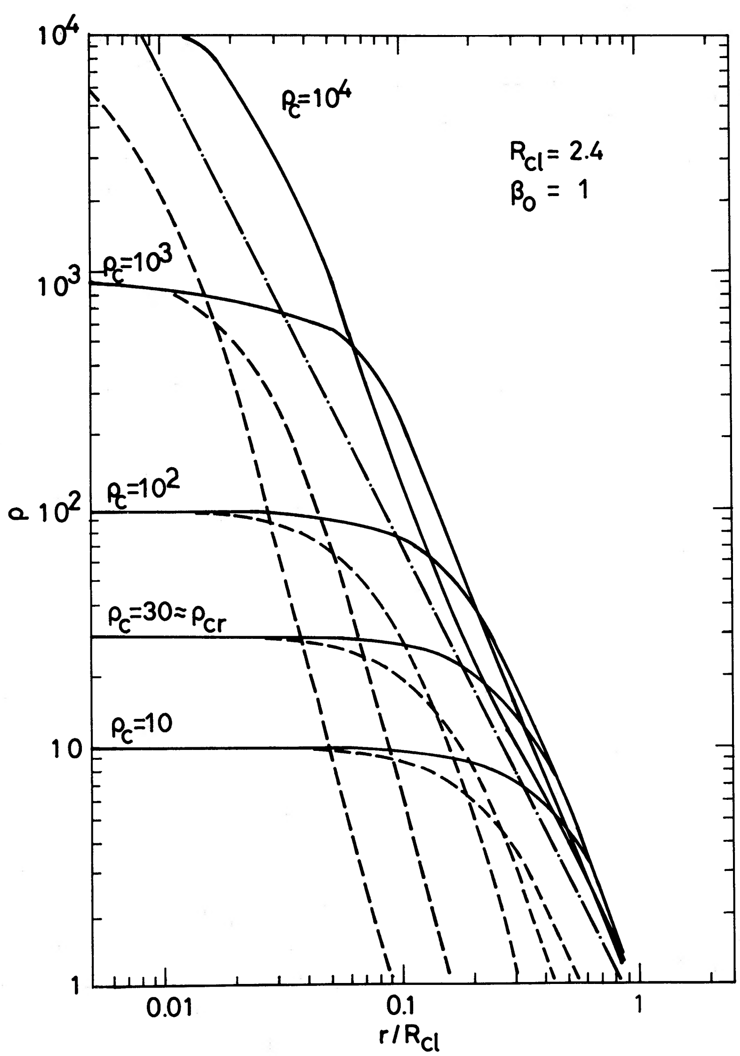

FIG. 2.—Density distributions along the r-axis ($z = 0$) and z-axis ($r = 0$) for clouds with $R_{cl} = 2.4$ and $\beta_0 = 1$. The cases with $\rho_c = 10$, 30, 10^2, 10^3, and 10^4 are plotted. The density at the equatorial plane $\rho(r)$ is shown by a solid line, and that on the z-axis $\rho(z)$ is shown by a dashed line. The "singular" distribution of the isothermal sphere is also shown in a dash-dot line.

system has no characteristic length scale. However, since the magnetized cloud has one characteristic length, i.e., R_{cl}, the absolute value of the density seems to be not exactly expressed by the "singular" distribution.

In Figure 3 the configurations of clouds with $R_{cl} = 2.4$ and $\beta_0 = 0.02$ are plotted. Comparing these with Figure 1, we can see the effect of the magnetic field on the shape of equilibria. Because of the strong field in the present case, the field line stays almost straight as long as $\rho_c \lesssim 30$. With increasing M_{cl} as well as increasing ρ_c, the magnetic field is squeezed near the equatorial plane. Because the cloud is supported laterally by the magnetic field, it is so hard for the cloud with stronger fields to collapse that the radius of the cloud, R_{fin}, for $\beta_0 = 0.02$ (Fig. 3) is larger than that for $\beta_0 = 1$ (Fig. 1). On the other hand, the height of the cloud, Z_{fin}, for $\beta_0 = 0.02$ is smaller than that for $\beta_0 = 1$, especially in the case of high density concentration, $\rho_c \gg 1$. This is due to the fact that the mass of the cloud with a strong magnetic field (small β_0) is larger than that with a weak field (large β_0) for given values of ρ_c (Tables 1 and 2).

The mass of the cloud, M_{cl}, for various values of ρ_c is shown in Table 1. The mass has a peak at $\rho_c \simeq 30$, increases monotonically for $\rho_c \lesssim 30$, and decreases monotonically for $\rho_c \gtrsim 30$ in the range we calculated. We show in Figure 4 the M_{cl}-ρ_c relation including other cases with different β_0. For comparison, the solution with $\beta_0 = \infty$ ($B_0 = 0$) is also shown, corresponding to the nonmagnetic spherical cloud. From this figure we can see the stability of magnetized clouds for global compression. When the cloud is compressed from the equilibrium state to a new state with $\rho_c' = \rho_c + \delta\rho_c$, in the case of $\partial M_{cl}/\partial\rho_c > 0$ this new ρ_c' state can support more mass than M_{cl}, so that this state is stable for compression. In contrast, in the case of $\partial M_{cl}/\partial\rho_c < 0$ the new ρ_c' state cannot support M_{cl}, and this equilibrium state is unstable for compression. Because the cloud mass is normalized by $p_{ext}^{1/2}(4\pi G)^{3/2}/c_s^4$, the cloud mass M_{cl} in the table is proportional to the square root of the external pressure. Table 1 shows that there is a maximum pressure beyond which clouds cannot exist stably, for a given value of mass.

TABLE 1

ADOPTED MODEL PARAMETERS (Fig. 1)

Case	β_0	R_{cl}	ρ_c	M_{cl}
a	1	2.4	2	42.6
b	1	2.4	3	58.2
c	1	2.4	5	73.1
d	1	2.4	10	84.9
e	1	2.4	30	89.9
f	1	2.4	10^2	86.7
g	1	2.4	10^3	76.2
h	1	2.4	10^4	75.8

TABLE 2

ADOPTED MODEL PARAMETERS (Fig. 3)

Case	β_0	R_{cl}	ρ_c	M_{cl}
a	0.02	2.4	2	47.3
b	0.02	2.4	3	68.2
c	0.02	2.4	5	93.1
d	0.02	2.4	10	127
e	0.02	2.4	30	183
f	0.02	2.4	10^2	239
g	0.02	2.4	10^3	283
h	0.02	2.4	10^4	279

The critical mass $M_{cr}(R_{cl}, \beta_0)$ which is defined as $\partial M_{cl}/\partial\rho_c = 0$ has an important meaning, that is, it is the maximum mass supported by thermal pressure and magnetic field. For mass larger than the critical mass, no equilibrium solution exists. The solution with $\partial M_{cl}/\partial\rho_c = 0$ corresponds to that called the "critical state" by Mouschovias (1976*b*). He could not find the solution on the branch $\partial M_{cl}/\partial\rho_c < 0$, because the solution is multivalued (at least two-valued) for a fixed M_{cl}. The cloud with $M_{cl} > M_{cr}(R_{cl}, \beta_0)$, which corresponds to that called the "supercritical cloud" by Shu, Adams, and Lizano (1987), is gravitationally unstable and collapses in a dynamical time scale.

b) The Cloud Mass

In Figure 4 the M_{cl}-ρ_c relations for $\beta_0 = 0$–5 are plotted. When the magnetic field becomes stronger, i.e., β_0 decreases, the critical mass M_{cr} increases, that is, the mass which can be supported by the magnetic field increases. Further, the density ρ_{cr} at which $\partial M_{cl}/\partial\rho_c = 0$ also increases for stronger magnetic field. Noticing that the solution with $\rho_c < \rho_{cr}$ is stable, we see that the stable region is extended much further for stronger magnetic field cases.

As seen in § III*a*, for the self-gravitating thin disk which is uniform in the *r*-direction the central density is expressed in terms of the column density along the *z*-direction as

$$\rho_c = \tfrac{1}{8}\sigma^2 + 1 , \tag{3.2}$$

where σ is normalized by $\sigma_0 = c_s[\rho_s/(4\pi G)]^{1/2}$. Using $\sigma \simeq \rho_i 2R_{cl} = 3M_{cl}/(2\pi R_{cl}^2)$, we can estimate the mass of the cloud in terms of ρ_c as

$$M_{cl} \simeq \frac{(4\sqrt{2})\pi}{3}(\rho_c - 1)^{1/2}R_{cl}^2 . \tag{3.3}$$

This approximate formula reproduces the results well for $\beta_0 = 0$ with $\rho_c \lesssim 10^3$ and for $\beta_0 \lesssim 0.02$ with $\rho_c \lesssim 10^2$ within 10%–20% errors. Because in the case with weak magnetic field the cloud collapses also in the *r*-direction and forms core, the thin-disk approximation becomes worse for weaker magnetic field. Comparing Figure 1*f* ($\beta_0 = 1$, $\rho_c = 10^2$) with Figure 3*f* ($\beta_0 = 0.02$, $\rho_c = 10^2$), we can see that the central part of the cloud becomes disklike with an increase in the strength of the magnetic field.

c) Effect of R_{cl}

In Figure 5 we plot the solution with $R_{cl} = 4.8$ and $\beta_0 = 1$. The size of the "parent cloud" is twice as large as that in Figure 1. The solution with $\rho_c \lesssim 50$ is stable for compression ($\partial M_{cl}/\rho_c > 0$), while that with $\rho_c \gtrsim 50$ is unstable ($\partial M_{cl}/\partial\rho_c < 0$). Compared with Figure 1, we clearly see that the cloud becomes globally geometrically thin. However, the half-thickness of the cloud decreases only by 20% from the solution with $R_{cl} = 2.4$ (note that Figs. 1 and 5 are plotted against r/R_{cl} and z/R_{cl}). This corresponds to the fact that z_b does not depend explicitly on R_{cl} as in equation (3.1). On the other hand, the cloud collapses slightly from the parent cloud in the *r*-direction. Therefore, the cloud becomes thin.

In Figure 6 the M_{cl}-ρ_c relation for $R_{cl} = 4.8$ is plotted. Comparing with Figure 4, we can see that $M_{cl}(\beta_0)$ is 2.3 times ($\beta_0 = 2$) to 3.3 times ($\beta_0 = 0.1$) as large as the values for $R_{cl} = 2.4$. The fact that, even when β_0 is fixed, M_{cr} increases for larger R_{cl} is explained by noting that the flux anchored to the cloud $[(\Phi_B)_{cl} \propto R_{cl}^2/\beta_0^{1/2}]$ increases with R_{cl}. Further, in accordance

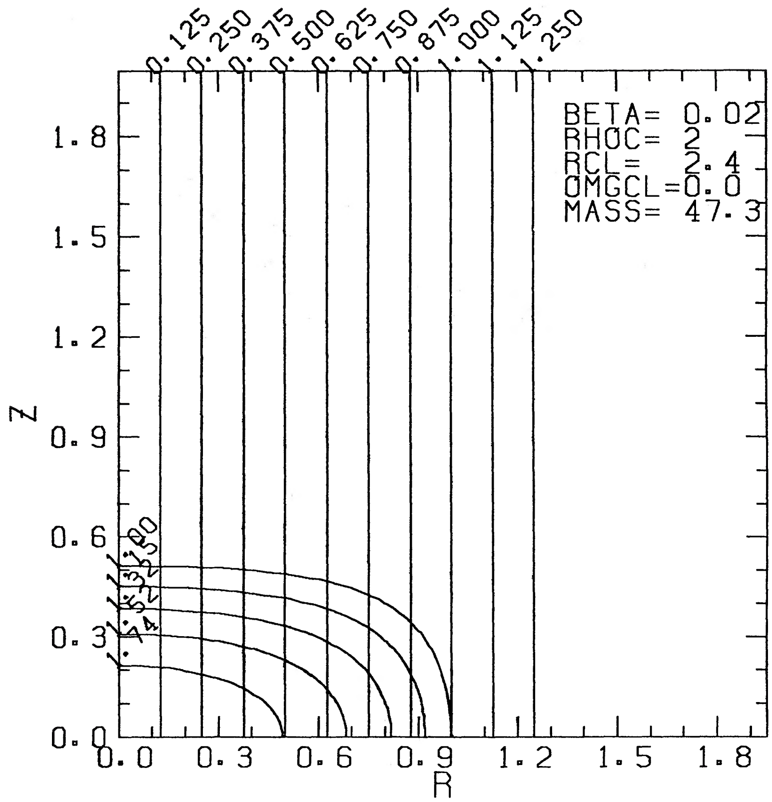

FIG. 3a

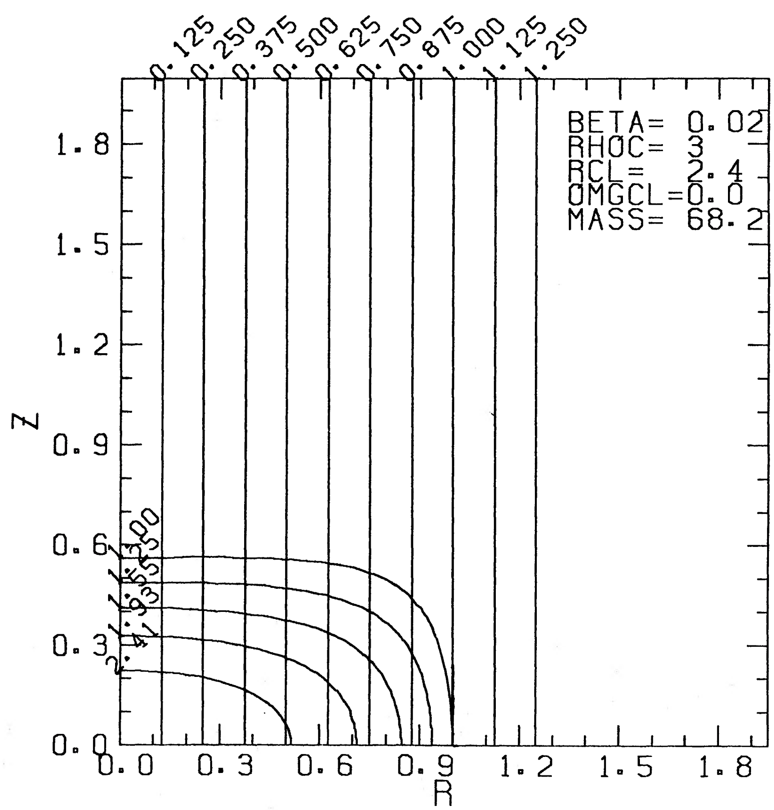

FIG. 3b

FIG. 3.—Same as Fig. 1, but for $\beta_0 = 0.02$. Parameters used here are shown in Table 2.

1988ApJ...335..239T

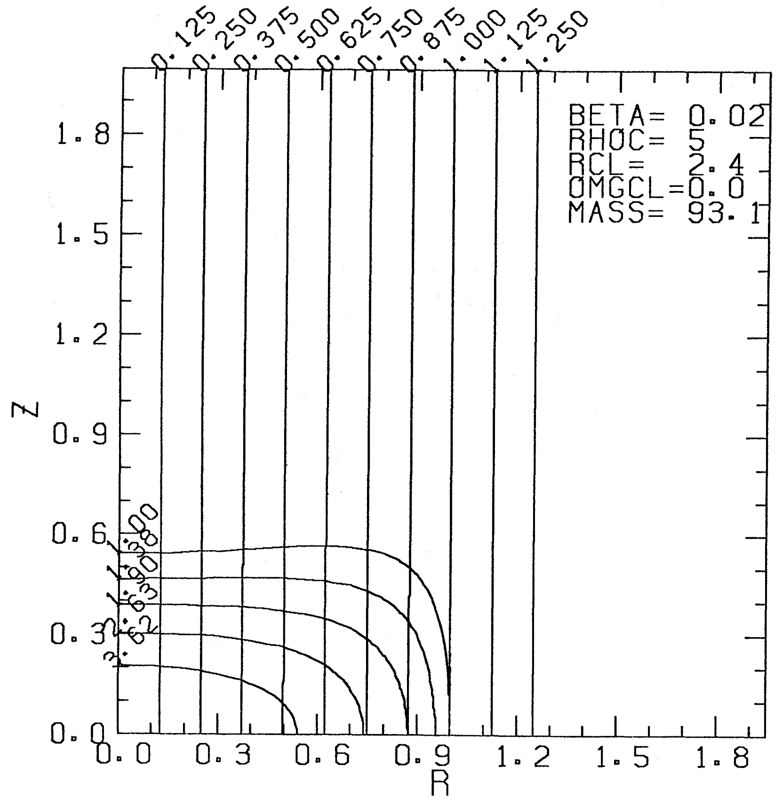

FIG. 3c

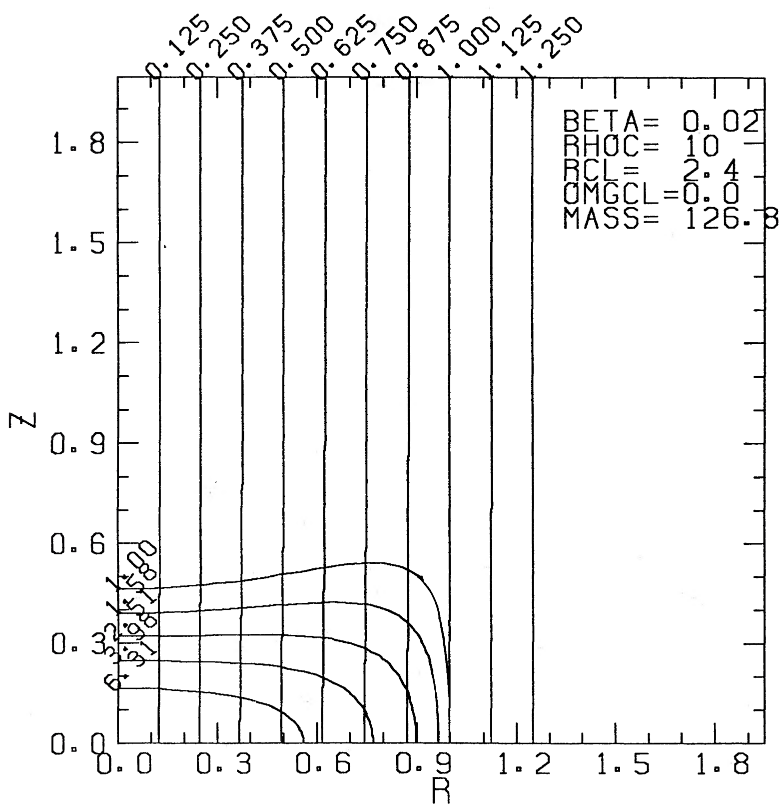

FIG. 3d

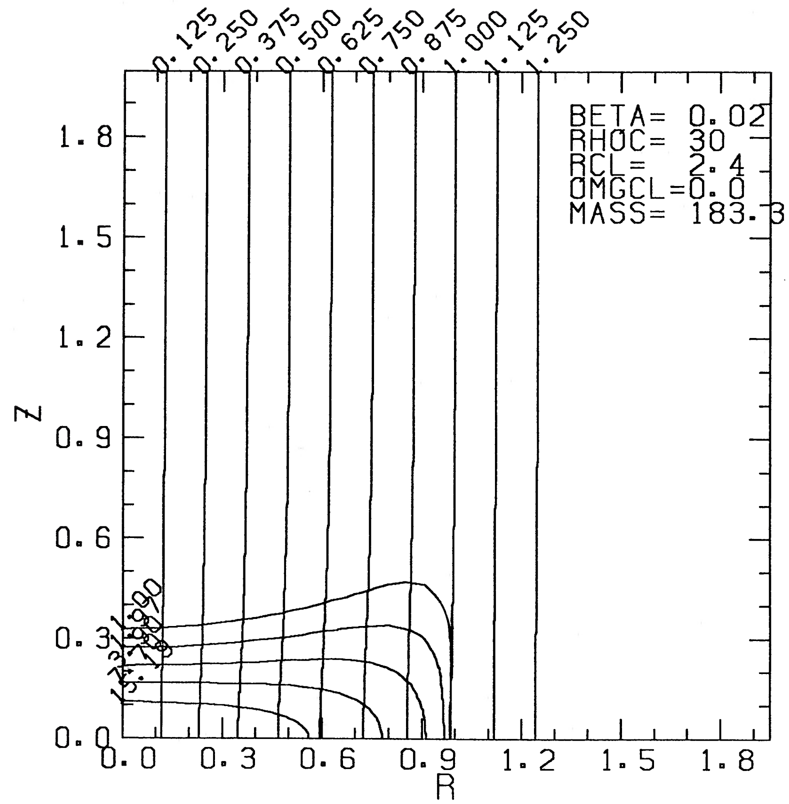
0.125
0.250
0.375
0.500
0.625
0.750
0.875
1.000
1.125
1.250
BETA= 0.02
RHOC= 30
RCL= 2.4
OMGCL=0.0
MASS= 183.3
Z
R
0.0
0.3
0.6
0.9
1.2
1.5
1.8

FIG. 3*e*

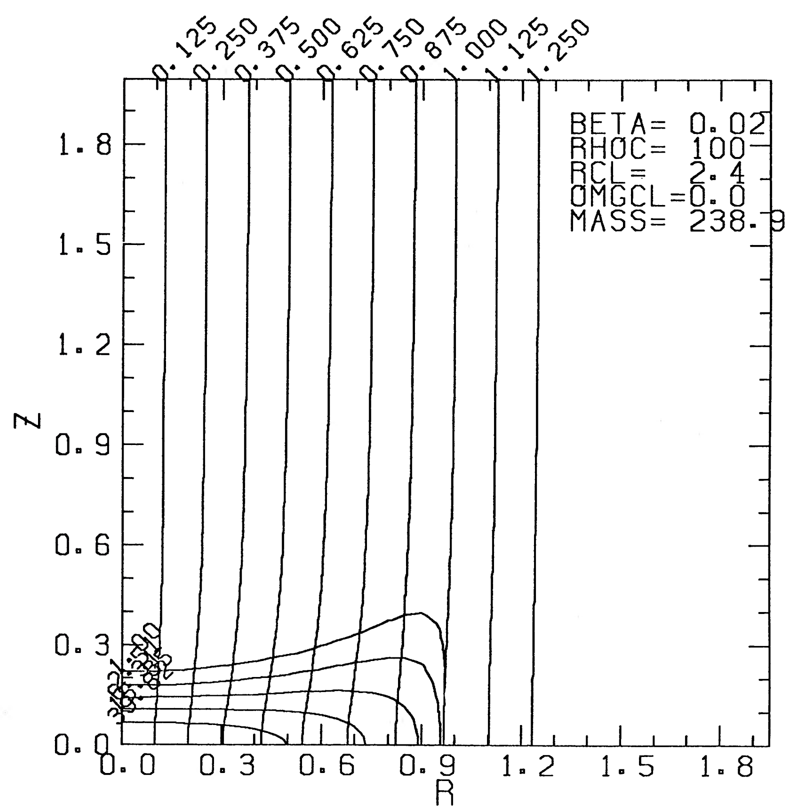
0.125
0.250
0.375
0.500
0.625
0.750
0.875
1.000
1.125
1.250
BETA= 0.02
RHOC= 100
RCL= 2.4
OMGCL=0.0
MASS= 238.9
Z
R
0.0
0.3
0.6
0.9
1.2
1.5
1.8

FIG. 3*f*

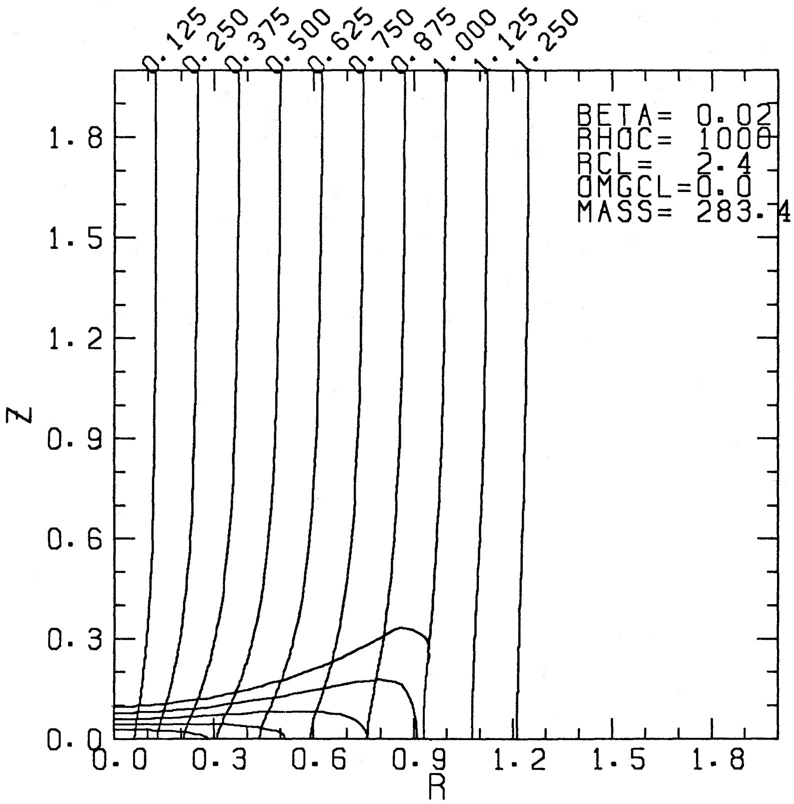
0.125
0.250
0.375
0.500
0.625
0.750
0.875
1.000
1.125
1.250
BETA= 0.02
RHOC= 1000
RCL= 2.4
OMGCL=0.0
MASS= 283.4
Z
R
0.0
0.3
0.6
0.9
1.2
1.5
1.8

FIG. 3*g*

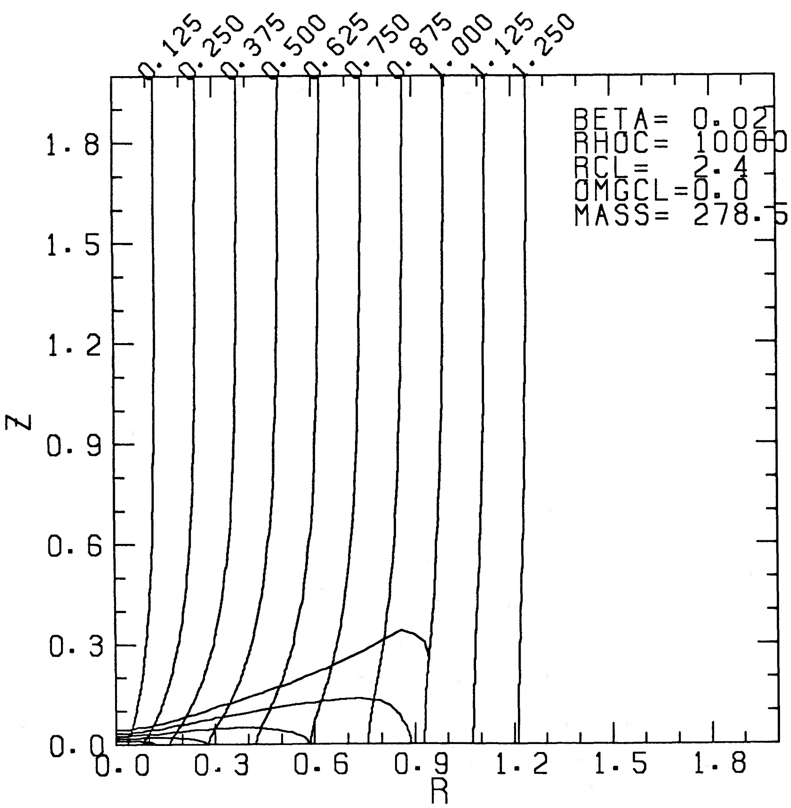
0.125
0.250
0.375
0.500
0.625
0.750
0.875
1.000
1.125
1.250
BETA= 0.02
RHOC= 10000
RCL= 2.4
OMGCL=0.0
MASS= 278.5
Z
R
0.0
0.3
0.6
0.9
1.2
1.5
1.8

FIG. 3*h*

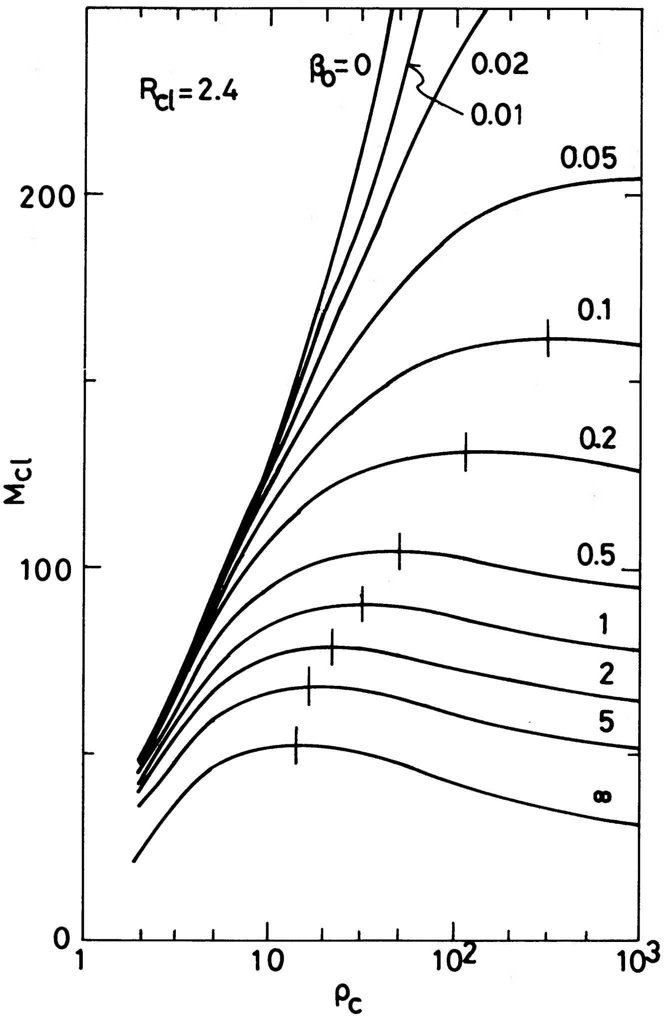

FIG. 4.—Mass of the cloud, M_{cl}, vs. central density, ρ_c, for various values of β_0. Except for $\beta_0 = 0$, M_{cl} takes a maximum value, which increases with increasing strength of the magnetic field B_0. The critical density, at which the mass reaches the maximum, also increases with increasing strength of the magnetic field.

with the increase in M_{cl}, the critical density ρ_{cr} becomes higher than that in Figure 4.

d) Effect of the Initial Mass Distribution

The distribution of mass with the magnetic flux seems to affect the equilibrium solution. To see this clearly, we compare the cases with $N = 0$ (Fig. 7*a*: cylindrical parent clouds), $N = 1$ (Fig. 7*b*: spherical parent clouds), and $N = 2$ (Fig. 7*c*: centrally condensed parent clouds), where we take other parameters fixed as $R_{cl} = 2.4$, $\beta_0 = 1$, and $\rho_c = 30$.

The equilibrium solution from the initial cylindrical cloud shows an almost cylindrical shape. Especially, the high-density disklike region conserves the initial shape. In contrast, in the case of the centrally condensed cloud, the global structure as well as the central high-density region shows a spherical shape. This is understood in such a way that the cloud mainly collapses parallel to the z-direction to form the equilibrium configuration, while in the r-direction the cloud is laterally supported by magnetic field.

In Figures 7*a*–7*c* we illustrate the results, respectively, of $M_{cl} = 99$ ($N = 0$), $M_{cl} = 90$ ($N = 1$), and $M_{cl} = 81$ ($N = 2$). The initial mass distribution with $N = 0$ can support a larger amount of mass than is the case for $N = 2$. In other words, with increasing central concentration, the mass supported by the magnetic field decreases. This seems to come from equation (2.5), i.e., $M_{cl}/(\Phi_B)_{cl}$ is proportional to the central mass-to-flux ratio $dm/d\Phi_B|_{\Phi_B=0}$,

$$\frac{M_{cl}}{(\Phi_B)_{cl}} = \frac{dm/d\Phi_B|_{\Phi_B=0}}{N/2+1}\,, \tag{3.4}$$

but is inversely proportional to $N/2 + 1$. At the center ($r \ll R_{cl}$), where the gravity is strong, even if $dm/d\Phi_B|_{\Phi_B=0}$ is the same irrespective of N, which will be shown later, the total mass depends upon N.

e) Magnetic Field at the Center

Mouschovias (1976*b*) pointed out that the magnetic field at the center of the cloud, B_c, and the central density ρ_c are well correlated. In Figure 8 we plot the relation between B_c and ρ_c for the cases shown in Figures 1, 3, and 5. This figure indicates a general trend,

$$B_c \propto \rho_c^{1/2}\,, \tag{3.5}$$

for higher central density. It is shown that this relation is realized over a wide range of parameters of ρ_c (10–10^4 for $\beta_0 = 1$; 100–10^4 for $\beta_0 = 0.02$). For lower density, however, B_c is independent of ρ_c. These results are simply explained by the thin-disk approximation. For a self-gravitating thin disk which is uniform in the r-direction, the central density is expressed as in equation (3.2) by

$$\rho_c \simeq \tfrac{1}{8}\sigma^2\,. \tag{3.6}$$

Now consider a flux tube threading the central region whose area is S. $S\sigma$ becomes proportional to M_{cl} from the conservation of mass in S. (1) Since $M_{cl} \sim M_{cr}$ for $\rho_c \gtrsim \rho_{cr}/5$, from equation (3.6) this implies $S \propto \rho_c^{-1/2}$. Since the magnetic field B_c is inversely proportional to S ($B_c S \simeq$ const), we obtain the above relation ($B_c \propto \rho_c^{1/2}$ for $\rho_c \gtrsim \rho_{cr}/5$). (2) For lower central density, the effect of magnetic fields is not so important, which implies $B_c \simeq B_0 =$ constant. The fact that the thin-disk approximation works well means that the gas density is almost constant along the r-axis near the central region of the magnetized cloud.

Here, we propose a fitting formula for the magnetic field strength at the center of the clouds:

$$\frac{B_c}{B_0} \simeq [1 + c\beta_0(\rho_c - 1)]^{1/2}\,, \tag{3.7}$$

where c is a parameter chosen to reproduce the results. We have confirmed that this equation with $c \simeq 0.5$ fits the numerical results within 20% relative error. Equation (3.7) is rewritten in a dimensional form as

$$\frac{B_c}{(4\pi\rho_c)^{1/2}} \simeq \left[\frac{B_0^2}{4\pi\rho_s}\frac{\rho_s}{\rho_c} + c_s^2\left(1 - \frac{\rho_s}{\rho_c}\right)\right]^{1/2}. \tag{3.8}$$

In the case of low central density $\rho_c/\rho_s \simeq 1$, the Alfvén speed at the center is equal to that at the outer part of the cloud. However, in the cloud with high central density, $\rho_c/\rho_s \gg 1$, the Alfvén speed at the center becomes nearly equal to the isothermal sound speed. In other words, the equipartition between magnetic energy and thermal energy proceeds.

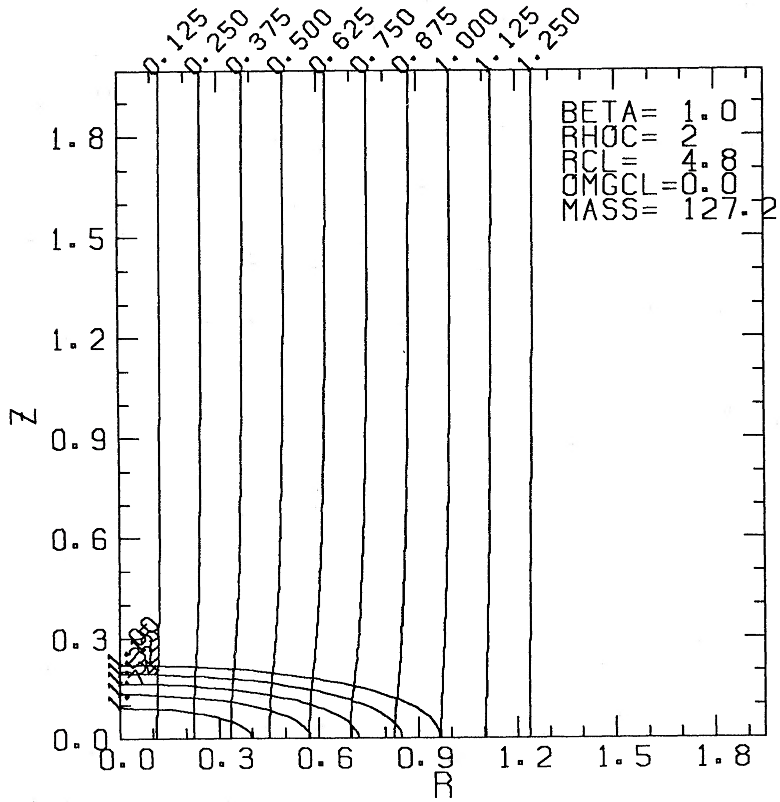

FIG. 5*a*

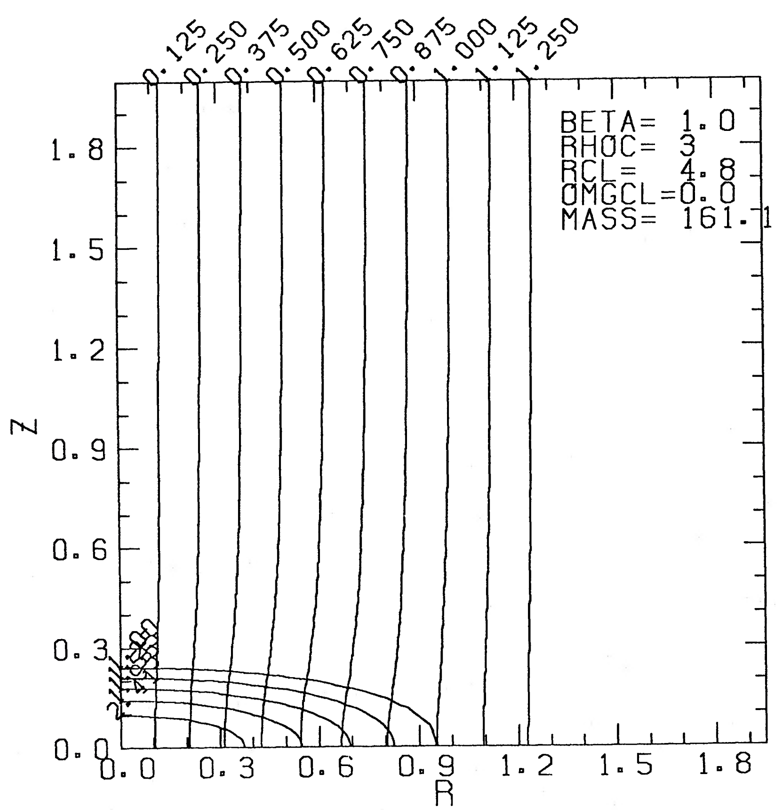

FIG. 5*b*

FIG. 5.—Same as Fig. 1, but for R_{cl} = 4.8. Parameters taken here are shown in Table 3.

1988ApJ...335..239T

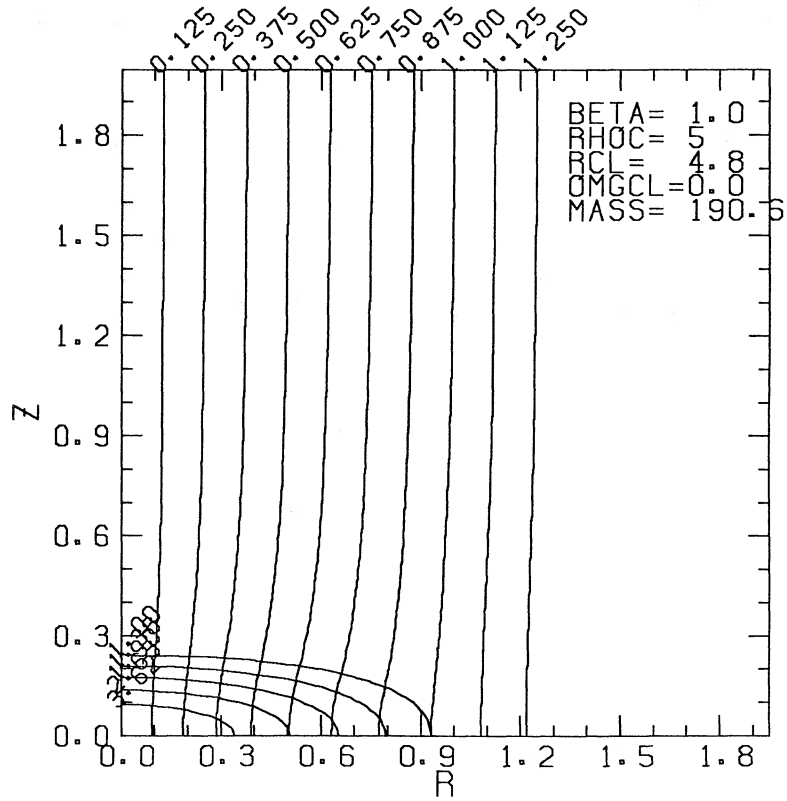

FIG. 5c

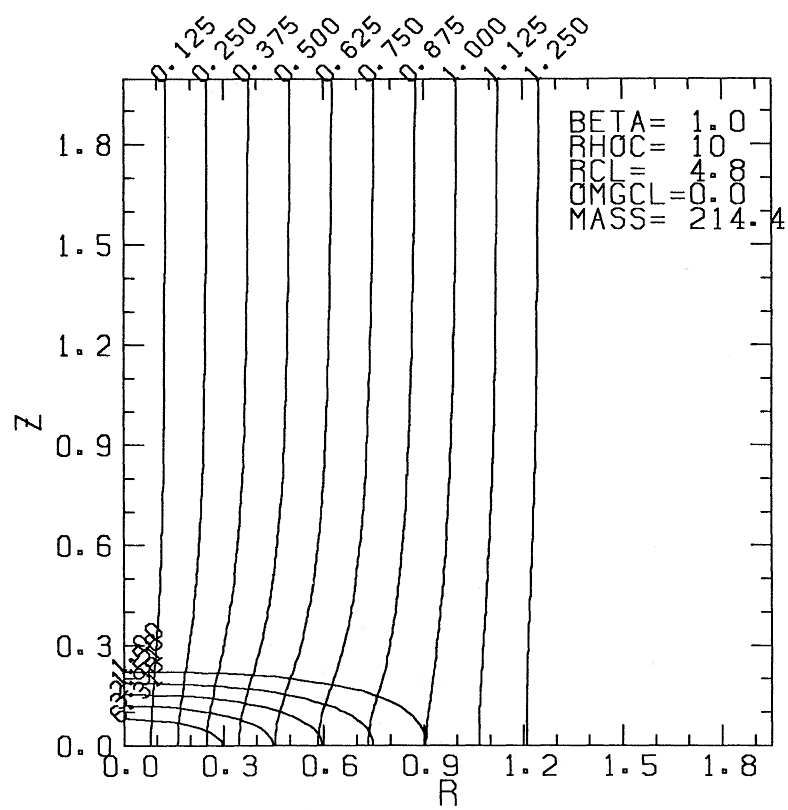

FIG. 5d

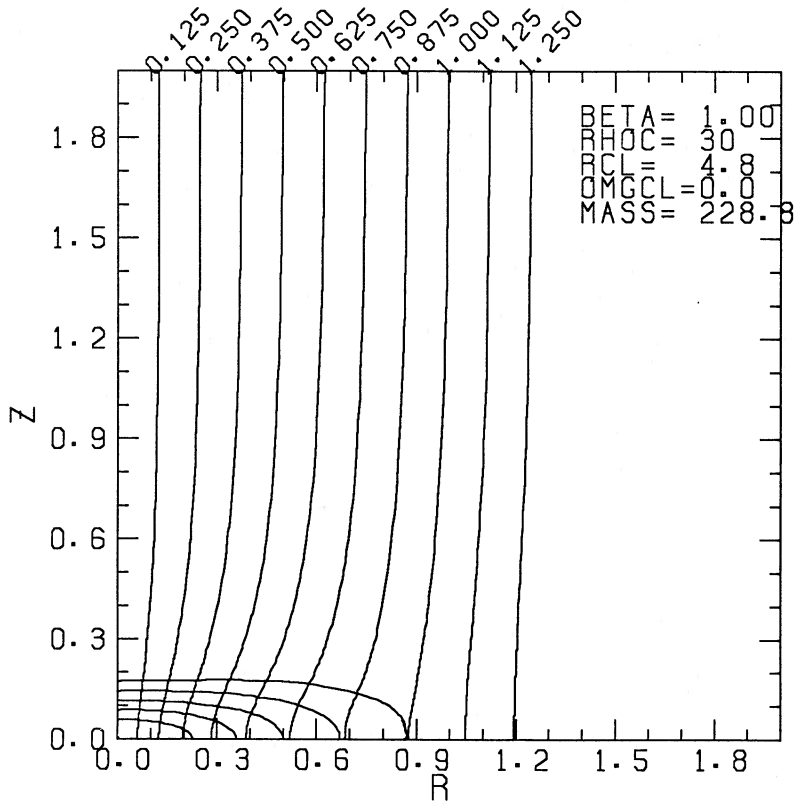
0.125
0.250
0.375
0.500
0.625
0.750
0.875
1.000
1.125
1.250
BETA= 1.00
RHOC= 30
RCL= 4.8
OMGCL=0.0
MASS= 228.8
Z
R

FIG. 5e

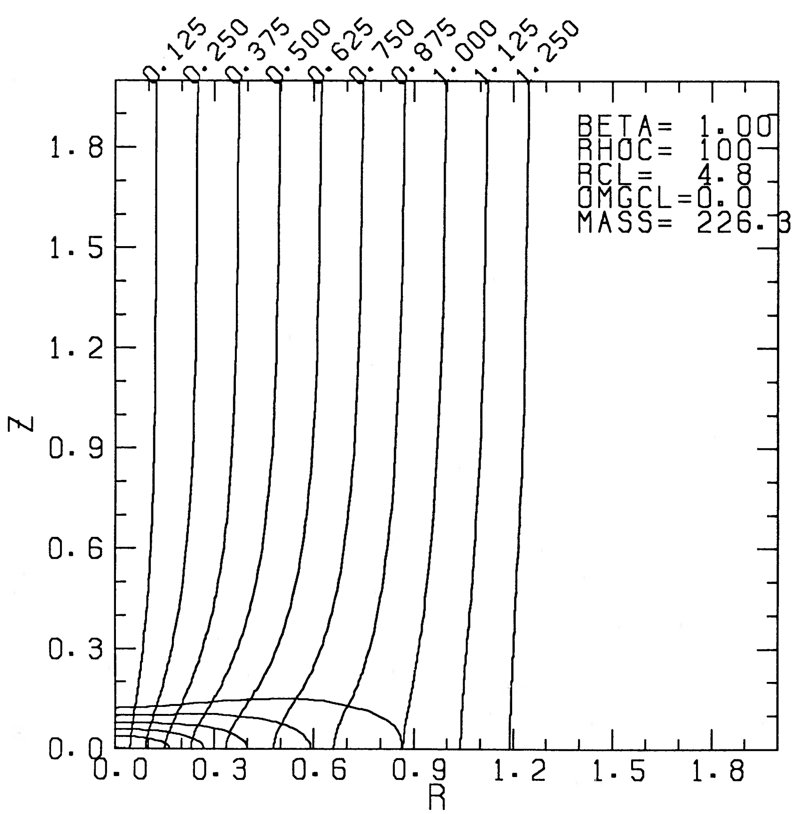
0.125
0.250
0.375
0.500
0.625
0.750
0.875
1.000
1.125
1.250
BETA= 1.00
RHOC= 100
RCL= 4.8
OMGCL=0.0
MASS= 226.3
Z
R

FIG. 5f

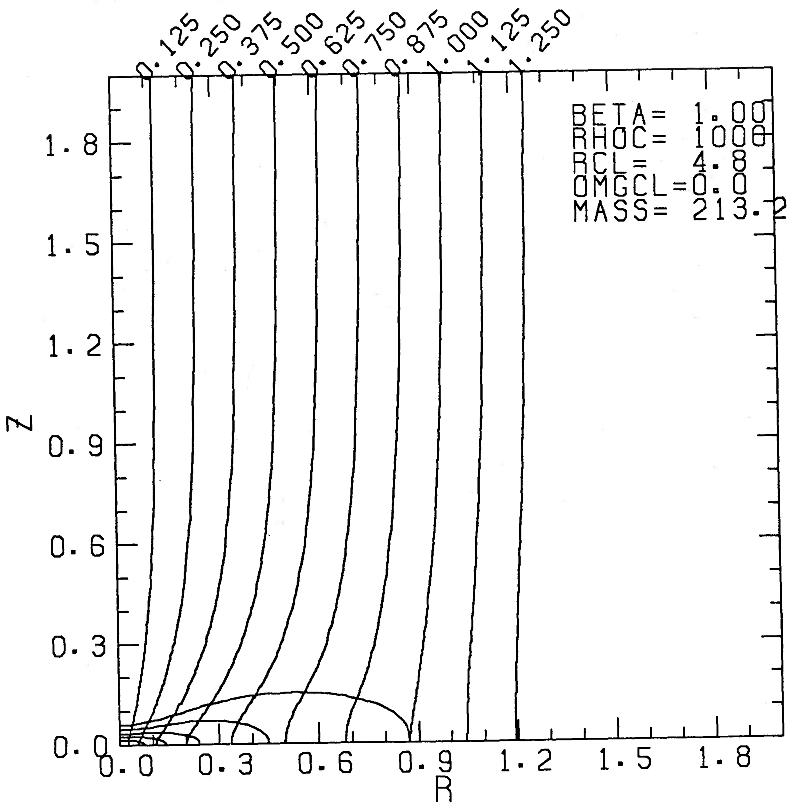
0.125
0.250
0.375
0.500
0.625
0.750
0.875
1.000
1.125
1.250
BETA= 1.00
RHOC= 1000
RCL= 4.8
OMGCL=0.0
MASS= 213.2
Z
R
0.0
0.3
0.6
0.9
1.2
1.5
1.8

FIG. 5*g*

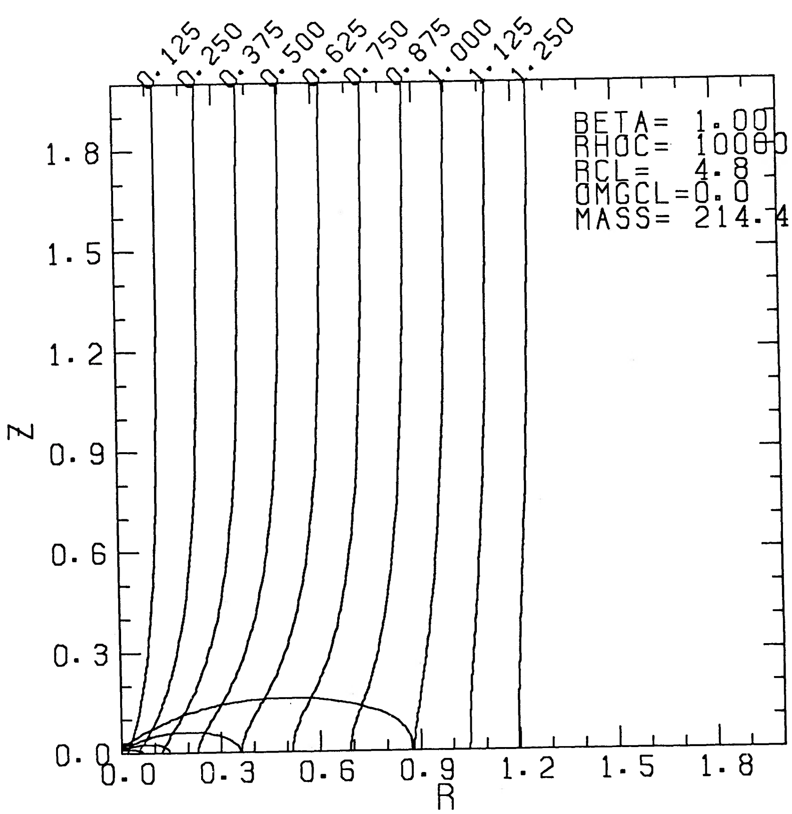
0.125
0.250
0.375
0.500
0.625
0.750
0.875
1.000
1.125
1.250
BETA= 1.00
RHOC= 10000
RCL= 4.8
OMGCL=0.0
MASS= 214.4
Z
R
0.0
0.3
0.6
0.9
1.2
1.5
1.8

FIG. 5*h*

TABLE 3

ADOPTED MODEL PARAMETERS (Fig. 5)

Case	β_0	R_{cl}	ρ_c	M_{cl}
a	1	4.8	2	127
b	1	4.8	3	161
c	1	4.8	5	191
d	1	4.8	10	214
e	1	4.8	30	229
f	1	4.8	10^2	226
g	1	4.8	10^3	213
h	1	4.8	10^4	214

IV. DISCUSSION

a) What Determines M_{cr} ?

In § III*c* it has been shown that the critical mass M_{cr} is an increasing function of the magnetic flux Φ_B. [Hereafter, we will represent the total magnetic flux $(\Phi_B)_{cl}$ by Φ_B for simplicity.] In this subsection we will see how M_{cr} is determined.

The ratio of mass to magnetic flux $M_{cl}/(\Phi_B/G^{1/2})$ stays constant as long as the frozen-in condition is applicable. Figure 9 shows the relation between the critical mass M_{cr} and the mass-to-flux ratio at the critical state, $M_{cl}/(\Phi_B/G^{1/2})|_{cr} \equiv M_{cr}\beta_0^{1/2}/[(4\sqrt{2})\pi R_{cl}^2]$. Dash-dot, solid, and dashed lines show, respectively, the solutions for cases with $N = 0$, $N = 1$, and $N = 2$. Each line corresponds to the change in M_{cr} for various β_0, i.e., with decreasing β_0 (increasing B_0) M_{cr} increases and the point in Figure 9 moves to the lower right.

When Φ_B is small enough (upper left-hand part of Fig. 9), M_{cr} is almost constant (60–100) irrespective of Φ_B. In the case of nonmagnetized spherical cloud, $M_{cr} = 52$ (note that the mass is normalized by $M_* \equiv c_s^4/[p_{ext}^{1/2}(4\pi G)^{3/2}]$). When Φ_B is taken large enough, the value of $M_{cl}/(\Phi_B/G^{1/2})|_{cr}$ seems to reach an asymptotic value irrespective of R_{cl}. The asymptotic values of $M_{cl}/(\Phi_B/G^{1/2})|_{cr}$ are different for different N, as $\simeq 0.17$ ($N = 0$), $\simeq 0.12$ ($N = 1$), and $\simeq 0.09$ ($N = 2$). That is, the magnetic field becomes less efficient in supporting the cloud as the concentration of the density to the center increases. In the use of equation (3.4), the asymptotic mass-to-flux ratio *at the center*

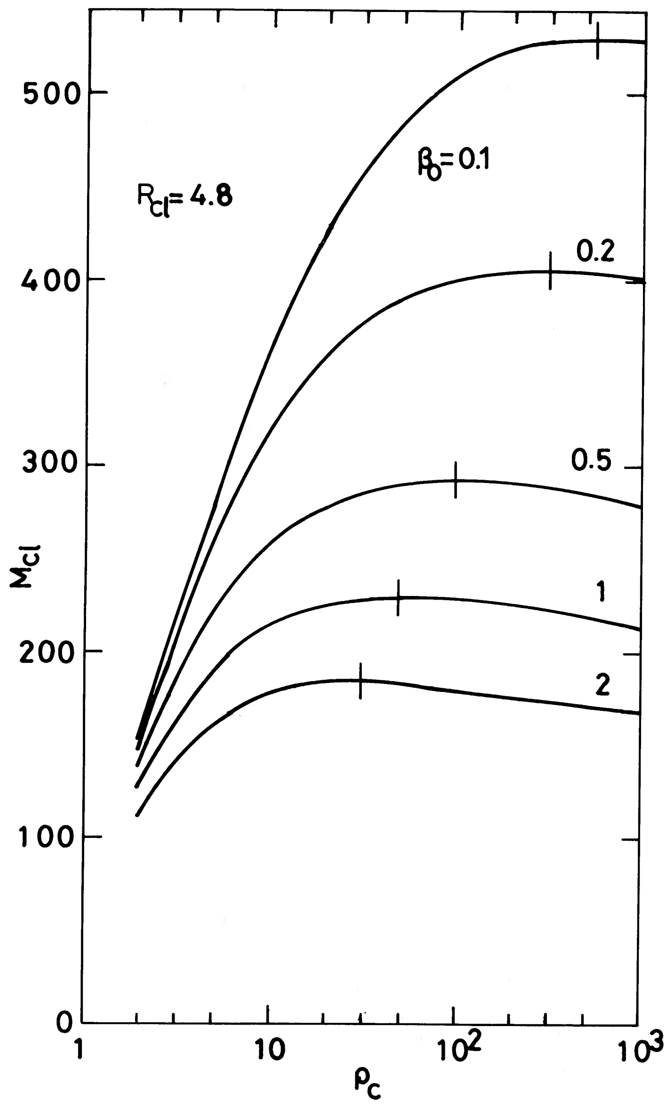

FIG. 6.—Same as Fig. 4, but for $R_{cl} = 4.8$

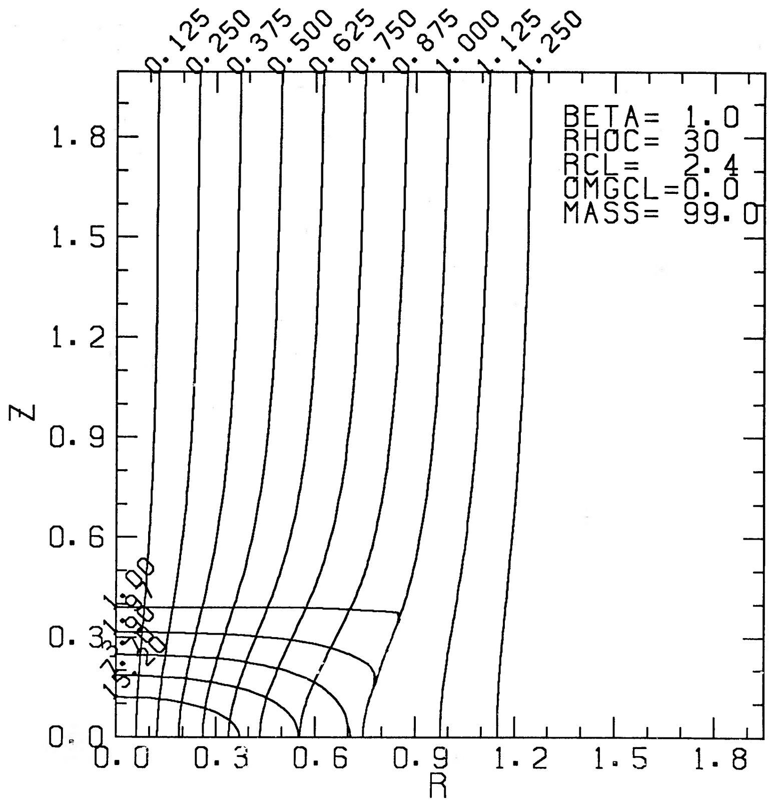

FIG. 7a

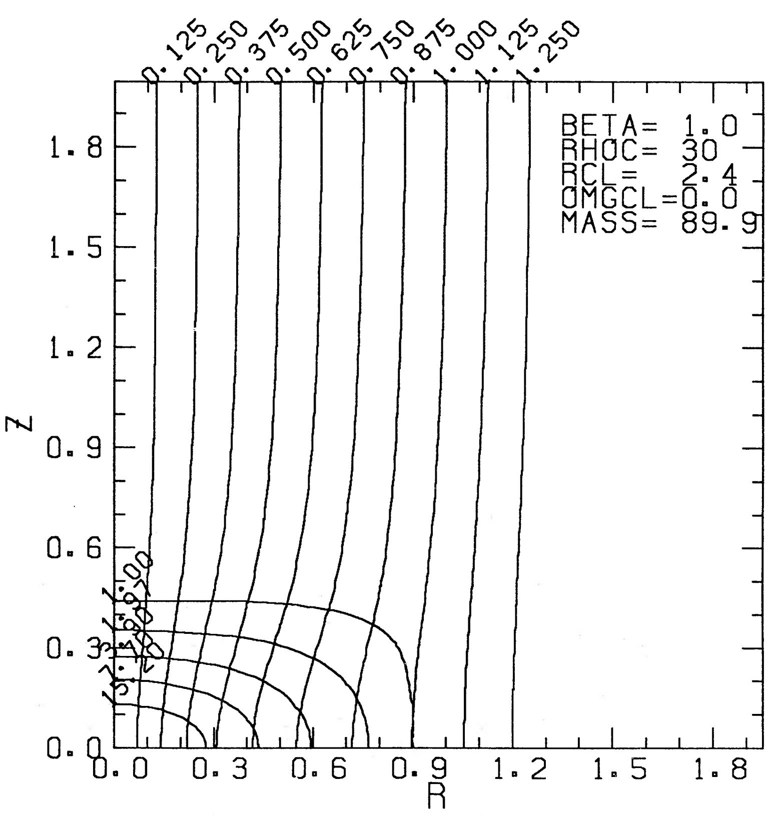

FIG. 7b

FIG. 7.—Comparison of the clouds with different initial density distributions. (*a*), (*b*), and (*c*) correspond to the "parent cloud," respectively cylindrical ($N = 0$), spherical ($N = 1$), and centrally condensed ($N = 2$). Parameters used here are shown in Table 4.

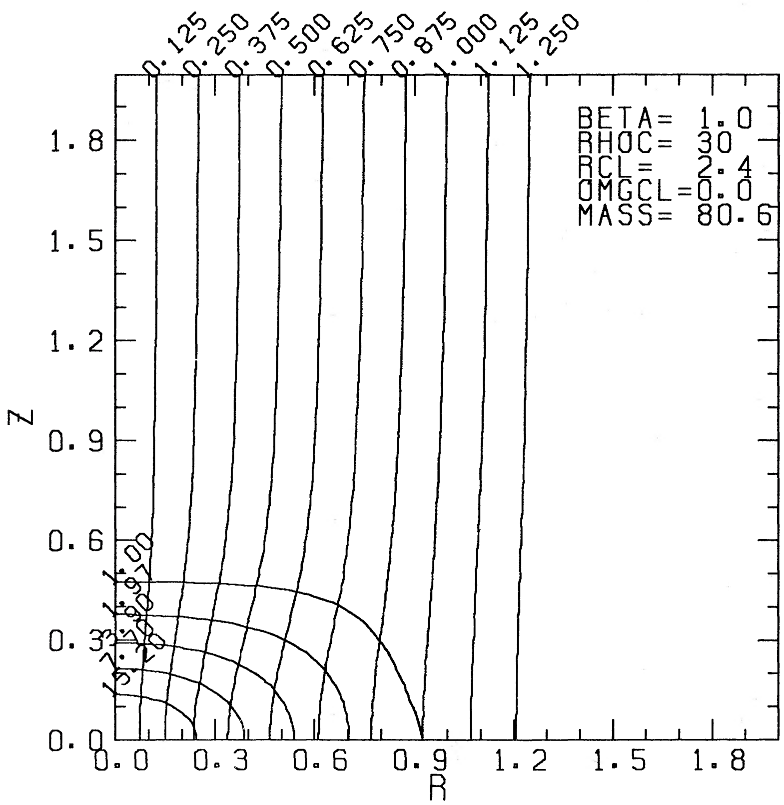

FIG. 7c

of the cloud becomes

$$\left.\frac{dm}{d\Phi_B/G^{1/2}}\right|_{r=0} \simeq \begin{cases} 0.17 & \text{for } N=0\,, \\ 0.18 & \text{for } N=1\,, \\ 0.18 & \text{for } N=2\,. \end{cases} \tag{4.1}$$

This shows that, irrespective of the initial mass distribution, the clouds whose mass-to-flux ratio at the center is greater than $\simeq 0.17$ are unstable for the strong magnetic field limit, while those whose mass-to-flux ratio at the center is less than $\simeq 0.17$ are stable.

b) Analysis Based on the Gibbs Free Energy

Here we try to understand the characteristics of the equilibrium solution by an analysis using the Gibbs free energy. In the case of a nonmagnetized spherical cloud (Lynden-Bell and Wood 1968), the *gravo-thermal* instability, which is characterized by the onset of negative specific heat at constant pressure $c_p < 0$ (Ebert 1957) (equivalently, the Gibbs free energy of the system takes a local *maximum*), occurs when $\partial M_{\rm cl}/\partial \rho_c < 0$. We suppose that the cloud with uniform density ρ, radius R, and mass M is threaded by the magnetic field B and confined by the external pressure p. The Gibbs free energy of this cloud is expressed as

$$\mathscr{G}(R, M) = Mc_s^2 \ln \rho - \frac{3}{5}\frac{GM^2}{R} + \frac{4\pi}{3} pR^3 + \frac{B^2R^3}{4}\,, \tag{4.2}$$

where the fourth term on the right-hand side, the magnetic energy, is taken from the model by Strittmatter (1966). This equation is rewritten using the magnetic flux $\Phi_B = \pi R^2 B$ as

$$\mathscr{G}(R, M) = Mc_s^2 \ln \rho - \frac{3G}{5R}\left(M^2 - \frac{5\Phi_B^2}{12\pi^2 G}\right) + \frac{4\pi}{3} pR^3\,. \tag{4.3}$$

We plot this free energy $\mathscr{G}$ as a function of R and M in Figure 10. The equilibrium point is found as a point where $\partial\mathscr{G}/\partial R = 0$. The stability of the equilibrium can easily be shown by taking the second derivative of $\mathscr{G}$:

$$\frac{\partial^2\mathscr{G}}{\partial R^2} > 0 \quad \text{for stable equilibrium} \tag{4.4a}$$

and

$$\frac{\partial^2\mathscr{G}}{\partial R^2} < 0 \quad \text{for unstable equilibrium}\,. \tag{4.4b}$$

From equation (4.3), we have the following three cases: (1) for $M < [5/(12\pi^2 G)]^{1/2}\Phi_B$, there is one stable equilibrium; (2) for $[5/(12\pi^2 G)]^{1/2}\Phi_B < M < \bar{M}$, the system has two equilibria: the one with larger R is stable and the other with smaller R is unstable; (3) for $M > \bar{M}$, there is no equilibrium solution, where $\bar{M}$ is determined from the condition $\partial\mathscr{G}/\partial R = \partial^2\mathscr{G}/\partial R^2 = 0$,

$$\frac{\bar{M}^2}{c_s^8/[(4\pi)^3 pG^3]} = \frac{3^4 5^3 \pi^2}{4^2}\left(1 - \frac{5\Phi_B}{\bar{M}^2 12\pi^2 G}\right)^{-3}. \tag{4.5}$$

TABLE 4

ADOPTED MODEL PARAMETERS (Fig. 7)

Case	N	β_0	$R_{\rm cl}$	ρ_c	$M_{\rm cl}$
a	0	1	2.4	30	99.0
b	1	1	2.4	30	89.9
c	2	1	2.4	30	80.6

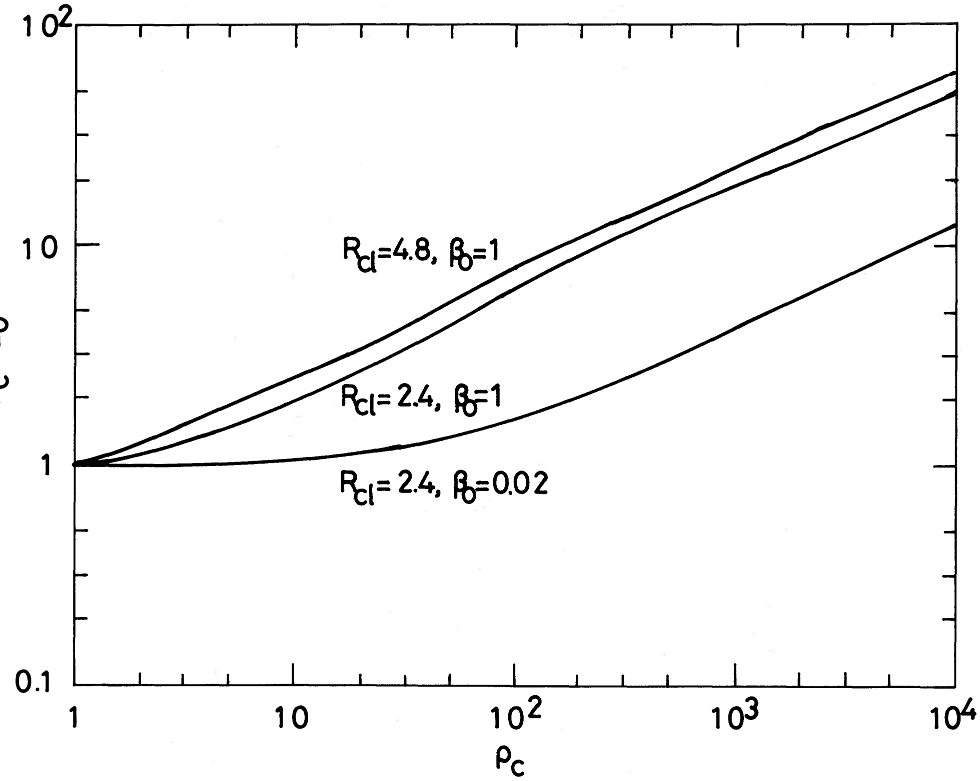

FIG. 8.—Relation between the magnetic field strength B_c and the density ρ_c at the center of the cloud. Three cases which are plotted in Figs. 1, 3, and 5 are presented.

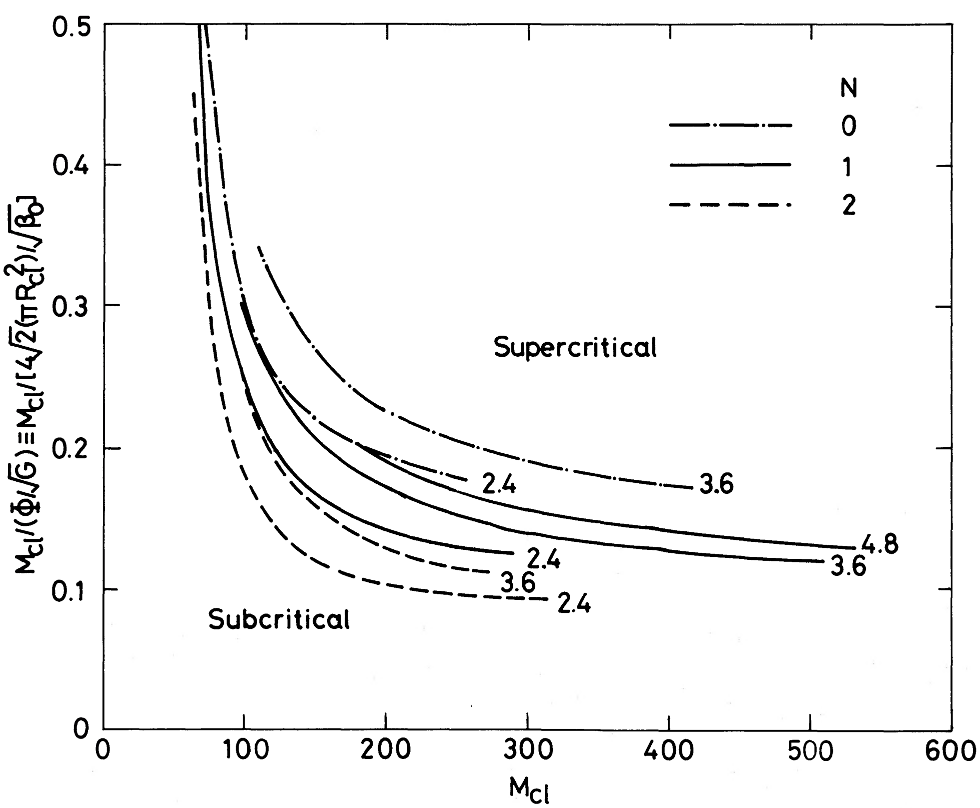

FIG. 9.—Relation between the critical mass of the cloud, M_{cr}, and the mass-to-flux ratio, $M_{cr}/(\Phi_B/G^{1/2})$. Dash-dot, solid, and dashed lines represent, respectively, the clouds with $N = 0$, $N = 1$, and $N = 2$. Along with the cases of $R_{cl} = 2.4$, results for the clouds with $R_{cl} = 3.6$ are also plotted. The result for $R_{cl} = 4.8$ is plotted only for $N = 1$.

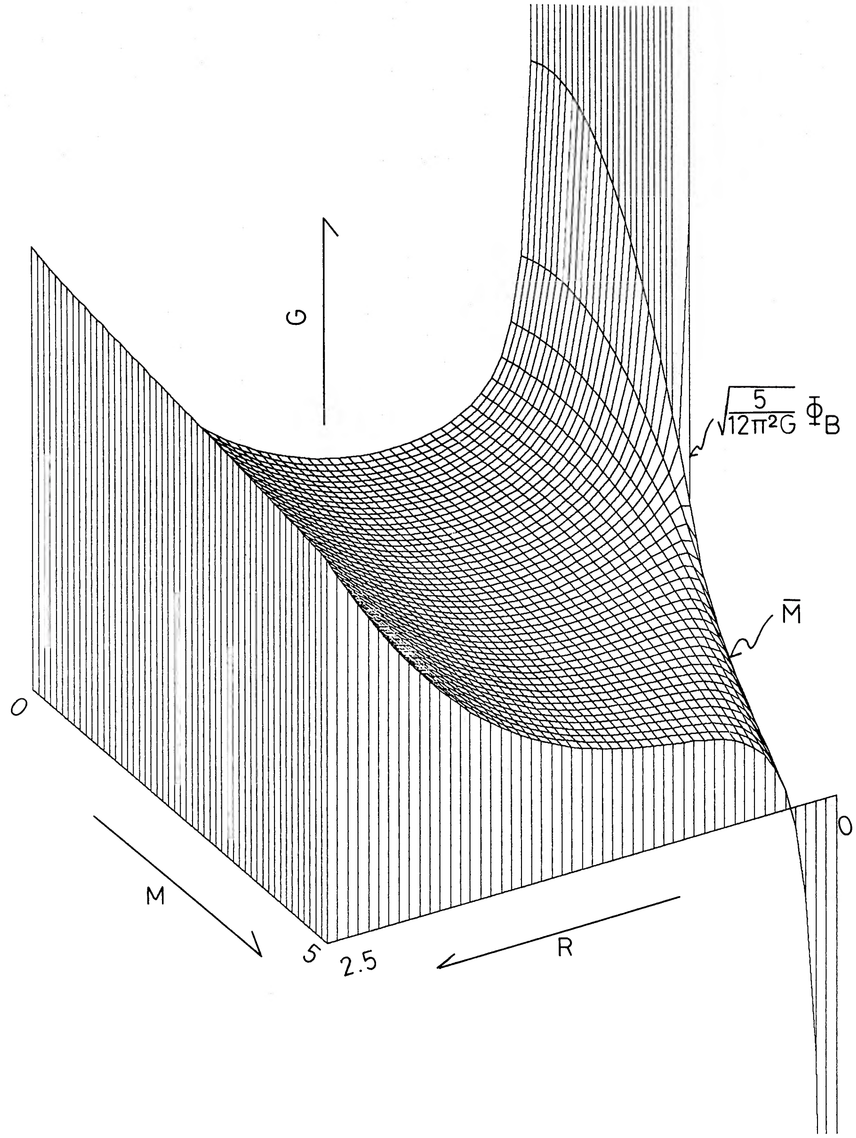

FIG. 10.—Three-dimensional view of the Gibbs free energy of the spherical uniform cloud with respect to radius R and mass M. Here, we take $[5/(12G)]^{1/2}\Phi_B/\pi = 2.5M_*$. In this case, the critical mass is $\bar{M} \simeq 3.908M_*$.

This is rewritten in nondimensional form as

$$\bar{M} = 79\left\{1 - \left[\frac{0.205}{\bar{M}/(\Phi_B/G^{1/2})}\right]^2\right\}^{-3/2} . \tag{4.6}$$

From this equation, it is easily shown that in the limit $\Phi_B \to 0$, $\bar{M}$ reduces to 79, and in the limit $\bar{M}/(\Phi_B/G^{1/2}) \to 0.205$, $\bar{M}$ increases infinitely. $\bar{M}$ is the mass above which no equilibrium solution exists. In this sense, $\bar{M}$ is equivalent to the critical mass which is determined as the mass where $\partial M_{cl}/\partial \rho_c = 0$. Thus, we regard $\bar{M}$ as identical with M_{cr}. If we replace the numerical factors in equation (4.6), e.g., 79 by 62, and 0.205 by 0.17, for $N = 0$, 0.12 for $N = 1$, and 0.09 for $N = 2$, then the numerical results in Figure 9 are reproduced within 10% error. Finally, using the mass-to-flux ratio at the center, the maximum mass is expressed *irrespective of N* as

$$M_{cr} = 62\left\{1 - \left[\frac{0.17}{dm/d(\Phi_B/G^{1/2})|_{r=0}}\right]^2\right\}^{-3/2} . \tag{4.7}$$

We can rewrite equation (4.7) in a useful form using the relation $dm/d\Phi_B = \sigma/B$:

$$M_{cr} \simeq 62\left\{1 - \left[\frac{0.17}{|\sigma/(B/G^{1/2})|_{r=0}}\right]^2\right\}^{-3/2} . \tag{4.8}$$

This means that when $|\sigma/(B/G^{1/2})|_{r=0} > 0.17$, there exists a finite maximum stable mass of cloud, M_{cr}, but when $|\sigma/(B/G^{1/2})|_{r=0} < 0.17$, there is no critical mass in equilibrium.

From the linear stability analysis of the self-gravitating isothermal slab extending infinitely in the x- and y-directions, Nakano and Nakamura (1978) and Tomisaka and Ikeuchi (1983) obtained the maximum stable column density of the slab as

$$\sigma_0 = \frac{B_0}{2\pi G^{1/2}} \simeq 0.16\,\frac{B_0}{G^{1/2}} , \tag{4.9}$$

where B_0 represents the magnetic field strength threading the slab perpendicularly. Further, when $\sigma_0/(B_0/G^{1/2}) > 1/(2\pi)$ the perturbation whose wavelength is longer than a critical wavelength, which corresponds to the Jeans wavelength, grows and makes the system unstable, but when $\sigma_0/(B_0/G^{1/2}) < 1/(2\pi)$ there is no unstable mode. Thus, correspondence between the equilibrium solution and the linear perturbation analysis is remarkable. This fact strengthens justification of the fitted form of the critical mass as equation (4.8).

There are two equilibria for $[5/(12\pi^2 G)]^{1/2}\Phi_B < M < \bar{M}$. This corresponds to the fact that in Figures 4 and 6 there are two different solutions with the same mass but different ρ_c. The stable equilibrium with large R in the free-energy analysis corresponds to the stable state with lower central density in the numerical solution, and the unstable equilibrium with small R corresponds to the unstable state with higher ρ_c.

From the above discussion, with increasing ρ_c keeping $M_{\rm cl}$ constant, the Gibbs free energy becomes a minimum at the stable equilibrium point and becomes a maximum at the unstable equilibrium point. Therefore, if a cloud is compressed by, e.g., cloud-cloud collision beyond the unstable equilibrium point, it becomes unstable and begins to collapse.

c) *Star Formation in Magnetized Clouds*

Here the condition for star formation is considered on the basis of the above analysis.

1. $M_{\rm cl} > M_{\rm cr}$.—The cloud whose mass exceeds $M_{\rm cr}$ is unstable from the initial stage. It collapses in a dynamical time scale if no support mechanism works other than thermal pressure and magnetic field. This cloud is situated in the upper right-hand region beyond the $M_{\rm cl} = M_{\rm cr}$ line in Figure 9; approximately, $M_{\rm cl} \gtrsim 100$ and $M_{\rm cl}/(\Phi_B/G^{1/2})|_{r=0} = \sigma/(B/G^{1/2})|_{r=0} \gtrsim 0.17$. These conditions are rewritten in dimensional form as

$$M_{\rm cl} \gtrsim 23\ M_\odot \left(\frac{T}{10\ \rm K}\right)^{3/2} \left(\frac{n_s}{100\ \rm H_2\ cm^{-3}}\right)^{-1/2}, \quad (4.10)$$

$$\sigma_{r=0} \gtrsim 0.02\ \rm g\ cm^{-2} \left(\frac{B}{30\ \mu G}\right). \quad (4.11)$$

Even when the cloud mass does not exceed $M_{\rm cr}$, accumulation of mass by collision seems to permit the cloud "supercritical" advocated by Shu (1987).

a) When the collision occurs in the direction of $\boldsymbol{B}$, the mass increases, keeping the magnetic flux constant. In Figure 9 the cloud moves to the upper right.

b) In the case in which collision occurs perpendicularly to $\boldsymbol{B}$, the mass increases, keeping the ratio M/Φ_B constant. The cloud moves to the right in Figure 9. In both cases, after the cloud crosses the critical line, it becomes unstable and star formation will proceed in a dynamical time scale.

2. $M_{\rm cl} < M_{\rm cr}$.—These clouds are stable. In addition to the mode described under condition 1, two other modes of triggering star formation will be contrived.

a) If the magnetic field escapes radially outward from the cloud because of the ambipolar diffusion (plasma drift), the total mass-to-flux ratio stays constant but that at the center rises. In Figure 9 the progress of the plasma drift drives the critical line to the lower left or, equivalently, increases N. If $M_{\rm cr}$ becomes less than the cloud mass, the cloud becomes unstable and collapses (Nakano 1979, 1982).

b) The cloud-cloud collision compresses the cloud efficiently. Even if the mass after merging of clouds does not exceed $M_{\rm cr}$, the cloud begins to collapse when it is compressed beyond the unstable equilibrium point by the collision. This is one of the modes of collision-induced star formation, which is studied numerically by Nagasawa and Miyama (1987) for nonmagnetized cloud collisions.

V. SUMMARY

We have succeeded in obtaining the equilibrium solutions of magnetized nonrotating clouds in a static external medium. From the solutions we have shown the following things:

1. There is a maximum mass $M_{\rm cr}$ which can be supported by a given magnetic flux. The maximum mass of the cloud is related to the mass-to-magnetic flux ratio at the center of the cloud (eq. [4.7]).

2. For $M_{\rm cl} < M_{\rm cr}$, we have found that there are two solutions with the same mass but different central density. One is the case with lower central density ρ_c, stable because of $\partial M_{\rm cl}/\partial\rho_c > 0$, and the other is the case with higher ρ_c, unstable with respect to the global compression because $\partial M_{\rm cl}/\partial\rho_c < 0$.

3. The stability of the cloud is well understood by a simple argument of the Gibbs free energy. The solution with $\partial M_{\rm cl}/\partial\rho_c > 0$ corresponds to the state with $\partial^2\mathscr{G}/\partial R^2 > 0$ and that with $\partial M_{\rm cl}/\partial\rho_c < 0$ corresponds to the state with $\partial^2\mathscr{G}/\partial R^2 < 0$.

4. The magnetic field strength and the central density of the cloud are well correlated according to $B_c \propto \rho_c^{1/2}$ for high central density. This means that in the central region the cloud has a disk shape—in other words, the density is almost constant along the r-direction.

5. The effect of the initial mass distribution on the maximum supported mass is studied. The maximum mass decreases with an increase in the central mass concentration N.

The numerical calculations were performed by FACOM M380-R at the National Astronomical Observatory, FACOM VP100 at the Institute of Space and Astronautical Sciences, and FACOM VP200 at the Data Processing Center, Kyoto University. This work was supported in part by a Grant-in-Aid for Science Research from the Ministry of Education, Science, and Culture (61790072 [K. T.], 62540178 [S. I.], and 62611517 [T. N.]). One of the authors (K. T.) acknowledges the JSPS Fellowships for Japanese Junior Scientists for financial aid in fiscal years 1986 and 1987.

REFERENCES

Chandrasekhar, S. 1957, *Stellar Structure* (New York: Dover), p. 155.
Ebert, R. 1957, *Zs. Ap.*, **42**, 263.
Harvey, P. M. 1985, in *Protostars and Planets II*, ed. D. C. Black and M. S. Matthews (Tucson: University of Arizona Press), p. 484.
Heiles, C. 1987, in *Interstellar Processes*, ed. D. J. Hollenbach and H. A. Thronson, Jr. (Dordrecht: Reidel), p. 171.
Heyer, M. H., Vrba, F. J., Snell, R. L., Schloerb, F. P., Strom, S. E., Goldsmith, P. F., and Strom, K. M. 1987, *Ap. J.*, **321**, 855.
Kiguchi, M., Narita, S., Miyama, S. M., and Hayashi, C. 1987, *Ap. J.*, **317**, 830.
Lynden-Bell, D., and Wood, R. 1986, *M.N.R.A.S.*, **138**, 495.
Mestel, L., and Ray, T. P. 1985, *M.N.R.A.S.*, **212**, 275.
Mouschovias, T. Ch. 1976*a*, *Ap. J.*, **206**, 753.
———. 1976*b*, *Ap. J.*, **207**, 141.
Mouschovias, T. Ch., and Spitzer, L. 1976, *Ap. J.*, **210**, 326.
Nagasawa, M., and Miyama, S. M. 1987, *Progr. Theoret. Phys.*, **78**, 1250.
Nakano, T. 1979, *Pub. Astr. Soc. Japan*, **31**, 697.
———. 1982, *Pub. Astr. Soc. Japan*, **34**, 337.
Nakano, T., and Nakamura, T. 1978, *Pub. Astr. Soc. Japan*, **30**, 671.

Shu, F. H. 1977, *Ap. J.*, **214**, 488.
———. 1987, in *Star Formation in Galaxies*, ed. C. J. L. Persson (NASA CP-2466), p. 743.
Shu, F. H., Adams, F. C., and Lizano, S. 1987, *Ann. Rev. Astr. Ap.*, **25**, 23.
Strittmatter, P. A. 1966, *M.N.R.A.S.*, **132**, 359.
Tamura, M., *et al.* 1987, in *IAU Symposium 115, Star Forming Regions*, ed. M. Peimbert and J. Jugaku (Dordrecht: Reidel), p. 48.
Tassoul, J.-L. 1978, *Theory of Rotating Stars* (Princeton: Princeton University Press), p. 169.
Tomisaka, K., and Ikeuchi, S. 1983, *Pub. Astr. Soc. Japan*, **35**, 187.
Tomisaka, K., Ikeuchi, S., and Nakamura, T. 1988, *Ap. J.*, **326**, 208 (Paper I).

SATORU IKEUCHI: National Astronomical Observatory, Mitaka, Tokyo 181, Japan

TAKASHI NAKAMURA: Department of Physics, Kyoto University, Kyoto 606, Japan

KOHJI TOMISAKA: Laboratory of Physics, Faculty of Education, Niigata University, Ikarashi 2-8050, Niigata 950-21, Japan